

Rotating Inertia Impact on Propulsion and Regenerative Braking for Electric Motor Driven Vehicles

By
Jeongwoo Lee

Thesis submitted to the Faculty of the
Virginia Polytechnic Institute and State University
in partial fulfillment of the requirements for the degree of
Master of Science
In
Mechanical Engineering

Committee members:

Douglas J. Nelson, Committee Chair
Michael W. Ellis
Charles F. Reinholtz

December 9, 2005
Blacksburg, Virginia

Key words: Drive Cycle, Regenerative Braking, Rotating Inertia, Vehicle Simulation

Copyright 2005, Jeongwoo Lee

Rotating Inertia Impact on Propulsion and Regenerative Braking for Electric Motor Driven Vehicles

Jeongwoo Lee

Abstract

A vehicle has several rotating components such as a traction electric motor, the driveline, and the wheels and tires. The rotating inertia of these components is important in vehicle performance analyses. However, in many studies, the rotating inertias are typically lumped into an equivalent inertial mass to simplify the analysis, making it difficult to investigate the effect of those components and losses for vehicle energy use. In this study, a backward-tracking model from the wheels and tires to the power source (battery or fuel cell) is developed to estimate the effect of rotating inertias for each component during propulsion and regenerative braking of a vehicle. This paper presents the effect of rotating inertias on the power and energy for propulsion and regenerative braking for two-wheel drive (either front or rear) and all-wheel drive (AWD) cases. On-road driving and dynamometer tests are different since only one axle (two wheels) is rotating in the latter case, instead of two axles (four wheels). The differences between an on-road test and a dynamometer test are estimated using the developed model. The results show that the rotating inertias can contribute a significant fraction (8 -13 %) of the energy recovered during deceleration due to the relatively lower losses of rotating components compared to vehicle inertia, where a large fraction is dissipated in friction braking. In a dynamometer test, the amount of energy captured from available energy in wheel/tire assemblies is slightly less than that of the AWD case in on-road test. The total regenerative brake energy capture is significantly higher (> 70 %) for a FWD vehicle on a dynamometer compared to an on-road case. The rest of inertial energy is lost by inefficiencies in components, regenerative brake fraction, and friction braking on the un-driven axle.

Acknowledgements

I would like to thank my academic and research advisor, Dr. Douglas Nelson for his continuous guidance, advice, patience and for presenting me a great opportunity to work on what I really wanted to do in Virginia Tech. I also would like to thank my thesis committee members, Dr. Ellis and Dr. Reinholtz for taking their time to review my Master's thesis. I especially thank to my family and relatives for their endless love and support to study in Virginia Tech. Last but not least, I want to thank my wife, Soyoun, who has supported and encouraged me to complete my Master's degree with her love.

Table of Contents

Abstract	ii
Acknowledgements	iii
Table of Contents	iv
Nomenclature	vi
List of Figures	viii
List of Tables	x
Chapter 1 Introduction	1
Chapter 2 Literature Review	3
2.1 Typical Vehicle Performance Analysis	3
2.2 Regenerative Braking Control Strategy in EV/HEV	4
2.3 Motor Sizing for EV/HEV	10
Chapter 3 Background Knowledge Applied to Simulation Model	13
3.1 Vehicle Forces	13
3.1.1 Tractive Force and Acceleration	13
3.1.2 Inertial Forces	18
3.2 Basic Idea of Rotating Inertia	20
Chapter 4 Simulation Model	22
4.1 Tractive Power	22
4.2 Propulsion	23
4.2.1 Power and Energy Required to Propel	23
4.2.2 Power Losses during Propulsion	27
4.2.3 Difference between on-road and dynamometer tests	27
4.3 Braking (Regenerative Braking)	28
4.3.1 Regenerative Brake Power and Energy	28
4.3.2 Power Losses during Regenerative Braking	33
4.4 Determination of Motor/Generator Efficiency	33
4.5 Acceleration Performance Analysis	35
4.6 Trace Miss Analysis	37
4.7 Specifications of Vehicle	39
Chapter 5 Results of Power and Energy over Various Drive Cycles	40
5.1 Propulsion Results over Drive Cycles	40

5.1.1 On-road Test	41
5.1.2 Dynamometer Test (Single Axle)	45
5.2 Braking (Regenerative Braking) Results over Drive Cycles	46
5.2.1 On-road Test	47
5.2.2 Dynamometer Test (Single Axle)	53
5.3 Net Energy Results	55
5.4 Comparison to Results with Two Different Effective Masses	57
5.5 Additional On-road Test Result for FWD	58
Chapter 6 Conclusion and Future Work	60
References	62
Appendix A: Motor/Controller Efficiency Data and Test Results	63
Appendix B: Drive Cycles	70
Vita	73

Nomenclature

A = Frontal area of a vehicle (m^2)	f_{rb} = Fraction of rear braking ($0 < f_{rb} < 1$)
a_i = Acceleration at i^{th} step (m^2)	G = Overall gear ratio
a_{i-1} = Acceleration at $i-1^{\text{th}}$ step (m^2)	g = Acceleration of gravity (m/s^2)
a_x = Longitudinal acceleration (m/s^2)	I = Moment of inertia ($kg\cdot m^2$)
C_D = Air drag coefficient	$I_{driveline}$ = Moment of inertia of driveline ($kg\cdot m^2$)
$C_{rr,front}$ = Rolling resistance coefficient of front wheels	$I_{M/G}$ = Moment of inertia of a motor/generator ($kg\cdot m^2$)
$C_{rr,rear}$ = Rolling resistance coefficient of rear wheels	$I_{w/t}$ = Moment of inertia of each wheel/tire assembly ($kg\cdot m^2$)
$E_{b,in}$ = Energy input into a battery by regenerative braking (J)	k = Regenerative braking fraction
$E_{b,out}$ = Energy output from a battery during propulsion (J)	M = Mass of a ring shape object (kg)
F_{aero} = Aerodynamic drag force (N)	m_{eff} = Effective mass of a vehicle (kg)
F_g = Resistance force by grade (N)	m_f = Fraction of mass on front axle
$F_{I,translation}$ = Translational inertial force (N)	m_t = Mass of a tire (kg)
$F_{I,t/w}$ = Rotating inertial force of four wheel/tire assemblies (N)	m_v = Total mass of test vehicle (kg)
F_p = Propulsive force (N)	m_w = Mass of a wheel (kg)
F_{rr} = Rolling resistance force of all wheels (N)	N_f = Final drive gear ratio
F_t = Tractive force for acceleration performance analysis (N)	N_t = Transmission gear ratio
F_{tow} = Towing force (N)	$P_{b,in}$ = Power input into a battery by regenerative braking (W)
F_{trac} = Tractive force at the ground (N)	$P_{b,out}$ = Power output from a battery to propel a vehicle (W)
f_b = Fraction of braking at driven axle ($0 < f_b \leq 1$)	$P_{brake,in}$ = Power input into brake system by braking (W)
f_{fb} = Fraction of front braking ($0 < f_{fb} < 1$)	$P_{driveline,in}$ = Power input into driveline by regenerative braking (W)
	$P_{driveline,out}$ = Power output from driveline to propel a vehicle (W)

$P_{M/G}$ = Power of M/G at output shaft (W)

$P_{M/G,in}$ = Power input into M/G by regenerative braking (W)

$P_{M/G,out}$ = Power output from M/G to propel a vehicle (W)

P_{trac} = Total tractive power required to propel a vehicle (W)

$P_{w/t,in}$ = Power input at ground by braking (W)

$P_{w/t,inertia}$ = Rotating inertial power of two wheel/tire assemblies (W)

$P_{w/t,out}$ = Power output from driven wheels to the ground (W)

R = Radius of a ring shape object (m)

r_r = Rolling radius of a wheel (m)

r_t = Outer radius of a tire (m)

r_w = Outer radius of a wheel (m)

$S_{M/G}$ = M/G speed at output shaft (rpm)

s_i = Cumulative distance at i^{th} step (m)

s_{i-1} = Cumulative distance at $i-1^{\text{th}}$ step (m)

Δs = Incremental distance traveled by the vehicle (m)

$T_{M/G}$ = Torque of M/G at output shaft (N-m)

t_i = Cumulative time at i^{th} step (sec)

t_{i-1} = Cumulative time at $i-1^{\text{th}}$ step (sec)

Δt = Incremental time (sec)

V = Vehicle speed (m/s)

V_{i-1} = Vehicle speed at $i-1^{\text{th}}$ step (m/s)

ΔV = Incremental speed of the vehicle (m/s)

η_t = Transmission efficiency

η_f = Final drive efficiency

$\eta_{M/G}$ = M/G efficiency

θ = Angle of the road from horizontal (rad)

ρ = Density of air (kg/m^3)

$\omega_{M/G}$ = Angular velocity of M/G at output shaft (rad/s)

List of Figures

Figure 2-1. Demonstration of parallel braking strategy	5
Figure 2-2. Regenerative brake force versus deceleration.....	6
Figure 2-3. Control logic of brake forces of front and rear wheels	7
Figure 2-4. Control logic of brake force distribution to regenerative and mechanical brake systems [7]...	8
Figure 2-5. Series regenerative braking strategy	10
Figure 2-6. Typical motor characteristics.....	11
Figure 3-1. Diagram of forces acting on a vehicle.....	14
Figure 3-2. Schematic diagram of a vehicle with ratios and rotating inertia at each component.....	17
Figure 3-3. Moment of inertia for a thin ring shape object.....	18
Figure 3-4. Basic concept of charging and discharging of rotating inertial power/energy	20
Figure 4-1. Power flow diagram of propelling for AWD vehicle.....	24
Figure 4-2. Power flow diagram of propelling for FWD vehicle.....	25
Figure 4-3. Power flow diagram of propelling for RWD vehicle	25
Figure 4-4. Power flow diagram of regenerative braking for AWD vehicle during braking	29
Figure 4-5. Power flow diagram of regenerative braking for FWD vehicle during braking.....	29
Figure 4-6. Power flow diagram of regenerative braking for RWD vehicle during braking	30
Figure 4-7. Trace miss flowchart	38
Figure 5-1. Energy distribution during propulsion over various drive cycles (on-road test)	41
Figure 5-2. Energy stored in rotating components during propulsion over a drive cycle (on-road test) ...	42
Figure 5-3. Energy flow during propulsion over drive cycles (on-road test)	44
Figure 5-4. Energy distribution during propulsion over various drive cycles (dynamometer test)	45
Figure 5-5. Energy stored in rotating components during propulsion over a drive cycle (dynamometer test)	46
Figure 5-6. Energy distribution during braking over various drive cycles (on-road test, AWD)	48
Figure 5-7. Energy distribution during braking over various drive cycles (on-road test, FWD)	48
Figure 5-8. Energy distribution during braking over various drive cycles (on-road test, RWD).....	49
Figure 5-9. Regenerative brake energy distribution during braking (on-road test, AWD)	50
Figure 5-10. Regenerative brake energy distribution during braking (on-road test, FWD).....	50
Figure 5-11. Regenerative brake energy distribution during braking (on-road test, RWD).....	51
Figure 5-12. Energy flow during braking over drive cycles (on-road test, AWD)	53
Figure 5-13. Energy distribution during braking over various drive cycles (dynamometer test)	54
Figure 5-14. Regenerative brake energy distribution during braking (dynamometer test).....	55

Figure 5-15. Net energy for on-road and dynamometer tests over various drive cycles.....	56
Figure 5-16. Regenerative brake energy capture comparison with the case using $f_{rb}=0.8$ and $k=0.8$ for on-road test with FWD over various drive cycles (UDDS cycle only).....	59
Figure 5-17. Net energy comparison with the case using $f_{rb}=0.8$ and $k=0.8$ for on-road test with FWD over various drive cycles.....	59
Figure B-1. UDDS cycle.....	70
Figure B-2. 505 cycle.....	70
Figure B-3. FTP cycle.....	71
Figure B-4. HWFET cycle.....	71
Figure B-5. US06 cycle.....	72

List of Tables

Table 4-1. Vehicle acceleration performance	37
Table 4-2. Mid-size SUV specifications	39
Table 4-3. Motor performance parameters	39
Table 5-1. Properties of drive cycles used in the analysis.....	42
Table 5-2. Fraction of energy loss at each component during propulsion (on-road test).....	43
Table 5-3. Fraction of energy loss at each component during braking (on-road test).....	52
Table 5-4. Comparison of cases with different constant mass factors to the primary test result (on-road test, AWD) (%)	58
Table A-1. Typical motor/controller efficiency data (%)	63
Table A-2. Energy required to propel the vehicle at each component over various drive cycles for AWD, FWD, and RWD (kJ)	64
Table A-3. Energy stored in rotating components due to rotating inertia at each component during propulsion over various drive cycles for AWD, FWD, and RWD (kJ).....	64
Table A-4. Energy loss at each component during propulsion over various drive cycles for AWD, FWD, and RWD (kJ).....	65
Table A-5. Regenerative brake energy at each component during braking over various drive cycles (kJ)	65
Table A-6. Energy recovered from rotating inertia at each component during braking over various drive cycles (kJ).....	66
Table A-7. Energy loss at each component during braking over various drive cycles (kJ).....	67
Table A-8. Net energy over drive cycles (kJ)	68
Table A-9. Other cases with different constant mass factors (on-road test, AWD) (kJ)	68
Table A-10. Regenerative brake energy at each component during braking over various drive cycles with higher fraction of front braking and regenerative brake fraction ($f_{fb}=0.8$ and $k=0.8$) (kJ).....	69
Table A-11. Energy recovered from rotating inertia at each component during braking over various drive cycles with higher fraction of front braking and regenerative brake fraction ($f_{fb}=0.8$ and $k=0.8$) (kJ)	69
Table A-12. Energy loss at each component during braking over various drive cycles with higher fraction of front braking and regenerative brake fraction ($f_{fb}=0.8$ and $k=0.8$) (kJ).....	69
Table A-13. Net energy over drive cycles with higher fraction of front braking and regenerative brake fraction ($f_{fb}=0.8$ and $k=0.8$) (kJ).....	69

Chapter 1

Introduction

Since the late 20th century, many automobile manufacturers and automotive engineers have focused on developing more efficient and powerful vehicles with reduced emissions. Along with those efforts and research, many new technologies have been developed, especially engine improvements such as gasoline direct injection, variable valve timing, variable compression ratio, turbocharging and supercharging. Besides the developments with conventional vehicles, new configurations and architectures for powertrains have been developed and introduced in the automotive industry, for example: hydrogen combustion engines, hybrid powertrains of gasoline or diesel engines with an electric traction motor, and fuel cell systems.

There are many useful simulation tools to analyze the performance of an electric motor driven vehicle. In a typical vehicle performance analysis, all components in a vehicle are often considered as one unit. For example, the entire vehicle is treated as one lumped mass in acceleration or deceleration performance analysis over various drive cycles. All inertias of rotating components such as a motor/generator (M/G), driveline, and assemblies of wheels and tires are lumped into an equivalent inertial mass and the combination of the equivalent mass and the mass of the test vehicle becomes an effective mass. In general, this effective mass is used for drive cycle analyses and its typical value is 1.03 – 1.05 times the mass for a conventional powertrain. Using the effective mass of the vehicle concentrated at its center of gravity (CG) is a convenient way to solve and model a complicated system. However, once all rotating inertias are lumped into the equivalent mass, the individual contributions are difficult to estimate in vehicle energy use analyses.

The objective of this study is to investigate and present the effect of rotating inertias on vehicle propulsion driven by an electric traction motor to obtain more accurate

power and energy estimates for both propulsion and regenerative braking. In this work, all the rotating components are classified into three major components and their inertias plus losses are evaluated respectively. The energy stored or discharged in rotating inertia is calculated over various drive cycles and included in propulsion power and energy equations. Also the power is tracked backward for each component from the wheel/tire assemblies to the power source (battery or fuel cell). In order to analyze power/energy flow during propulsion and braking, a backward tracking model is developed and five drive cycles are tested: UDDS, 505, FTP, HWFET, and US06 [1].

In this analysis, all wheel drive (AWD), and single axle drive (FWD or RWD) vehicles are simulated for five drive cycles for both on-road and dynamometer tests. Note that a dynamometer test is different from an on-road test, because only one axle is spinning on a dynamometer and it reduces the rotating inertia of wheel/tire assemblies. The differences are explained in detail in later sections.

In this paper, a pure battery electric powertrain is presented, but the analysis is applicable to hybrid and fuel cell powertrains as well. In this study, a non-slip condition between wheels and tires is assumed for all analyses.

Chapter 2

Literature Review

2.1 Typical Vehicle Performance Analysis

In a vehicle acceleration performance analysis, the test vehicle mass is not directly used for acceleration analysis since a moving vehicle has both translational inertia and rotating inertia during acceleration or deceleration. Therefore, the actual mass used for analysis could be significantly larger than the test vehicle mass. A vehicle has many rotating components and they have rotating inertias. As mentioned earlier in the introduction, all those rotating components in a vehicle are often considered as one unit in a typical vehicle performance analysis. Many text books related to vehicle performance analysis explain how to lump such rotating inertias into the inertial mass or the effective mass [2, 3, 4].

Miller [3] shows an example analysis using the rotating inertia of many rotating components for the effective mass in the first chapter of his book. All the rotating components such as a crank shaft, torque converter, impeller and turbine, gear, and wheels are considered and their rotating inertias are lumped into the effective mass. In this example analysis, the result shows that the contribution of small rotating components are very small, but the effect of rotating inertia is almost the same as adding up one passenger's weight depending on the size of rotating components. Thus, the effect on fuel economy is not negligible.

Sovran and Blaser [5], use the rotating inertia of wheels to calculate the tractive force of the vehicle in their research. The tractive force equation they use is shown below.

$$\begin{aligned}
F_{TR} &= R + D + \left(M + 4 \left[\frac{I_w}{r_w^2} \right] \right) \left(\frac{dV}{dt} \right) \\
&= \underbrace{r_0 M g}_{\text{tire resistance}} + \underbrace{C_D A \frac{V^2}{2} \rho}_{\text{aerodynamic drag}} + \underbrace{\left(M + 4 \left[\frac{I_w}{r_w^2} \right] \right)}_{\text{linear+rotational inertia}} \left(\frac{dV}{dt} \right)
\end{aligned} \tag{2-1}$$

The last term in equation (2-1) is the effective mass term which includes the linear inertia (or translational inertia) and the rotating inertia of the four wheels. In this study, they only consider wheels as a rotating component for the effective mass and the rotating inertia of the power train is considered as part of powertrain. More detailed explanation is presented in Chapter 3.

2.2 Regenerative Braking Control Strategy in EV/HEV

The brake energy would normally be dissipated and wasted as heat during braking in a conventional vehicle. Thus vehicles driven by a electric traction motor, such as HEVs, EVs and fuel cell electric vehicles (FCVs), have a regenerative brake system to improve the fuel economy and the braking split between the driven and non-driven axles may vary the overall efficiency of the vehicle.

In an EV and HEV, only the driven axle can capture the regenerative brake energy and the rest of the brake energy is dissipated as heat by friction braking on both the driven and the un-driven axle. Gao et al [6], investigate the effectiveness of regenerative braking for FWD EV and HEV with three different patterns of braking.

1. If the required brake force on the front axle does not exceed the maximum regenerative brake force available, then only regenerative brake force is applied to the front axle and a proper amount of frictional brake force on the rear axle is applied to maintain stability or avoid a wheel lock-up.
2. If the required brake force on the front axle exceeds the maximum regenerative brake force available, then both the regenerative brake and

mechanical brake forces are applied to the front axle and a proper amount of frictional brake force on the rear axle is applied to avoid a wheel lock-up.

3. In a relatively small deceleration, for example deceleration of less than 0.3g, and the available regenerative brake force can meet the demand, only regenerative brake force is applied to the front axle, and no frictional brake force is applied to both front and rear axles.

As shown above, the regenerative brake force is effective only for the front axle. They build a parallel braking control strategy based on this scheme which is shown in Figure 2-1. In the figure, the shaded region is the regenerative brake force applied on the front axle. Figure 2-2 shows the regenerative brake force along the deceleration.

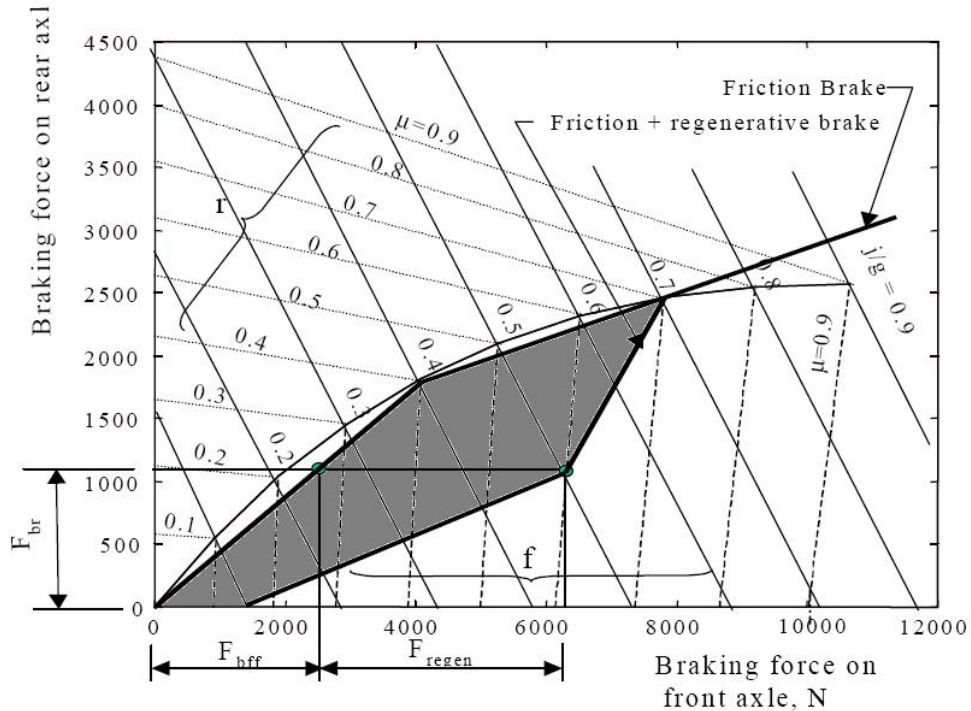


Figure 2-1. Demonstration of parallel braking strategy [6]

(Reprinted with permission from SAE Paper 1999-01-2910 © 1999 SAE International)

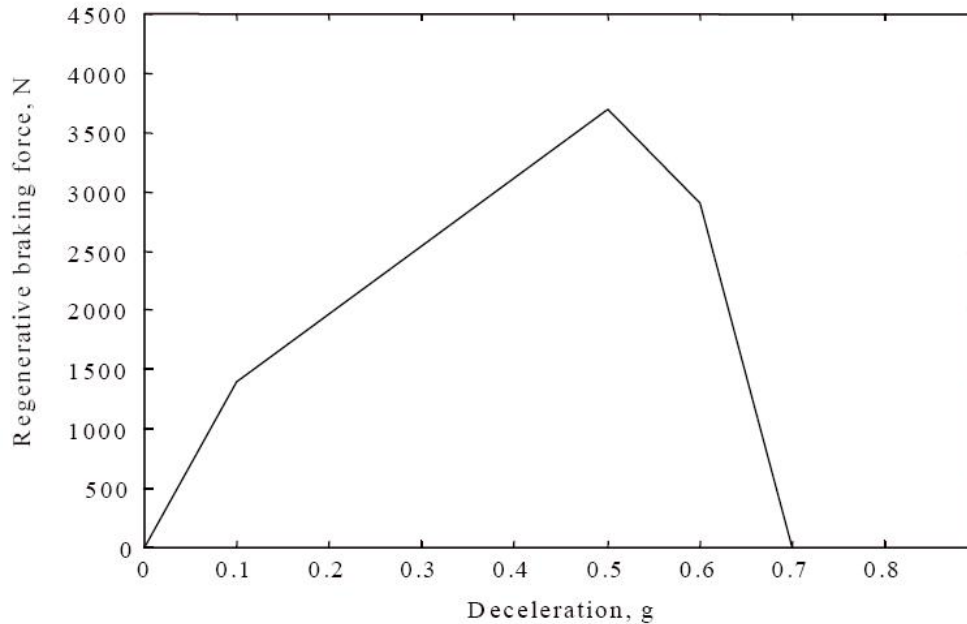


Figure 2-2. Regenerative brake force versus deceleration [6]

(Reprinted with permission from SAE Paper 1999-01-2910 © 1999 SAE International)

They use the regenerative brake control strategy as shown in Figures 2-1 and 2-2. According to their results, significant amount of total brake energy (63 - 100%) could be recovered in urban driving cycles.

However, it is impossible to recover 100% of brake energy in reality, since there are losses by mechanical inefficiencies and some other factors. Thus, later on, Gao and Ehsani [7], develop strategies for controlling the brake forces between the frictional and regenerative brakes on front and rear axles to recover more energy by regenerative braking and achieve a safe brake system as a conventional vehicle. Figures 2-3 and 2-4 show the control strategies of brake force of front and rear wheels, and brake force distribution between regenerative and mechanical brake systems. Using those control strategies of brake forces, the simulation results show that more than 60% of brake energy can be recovered in typical urban drive cycles. Note that the simulation is performed with a vehicle that only front axle is available for regenerative braking.

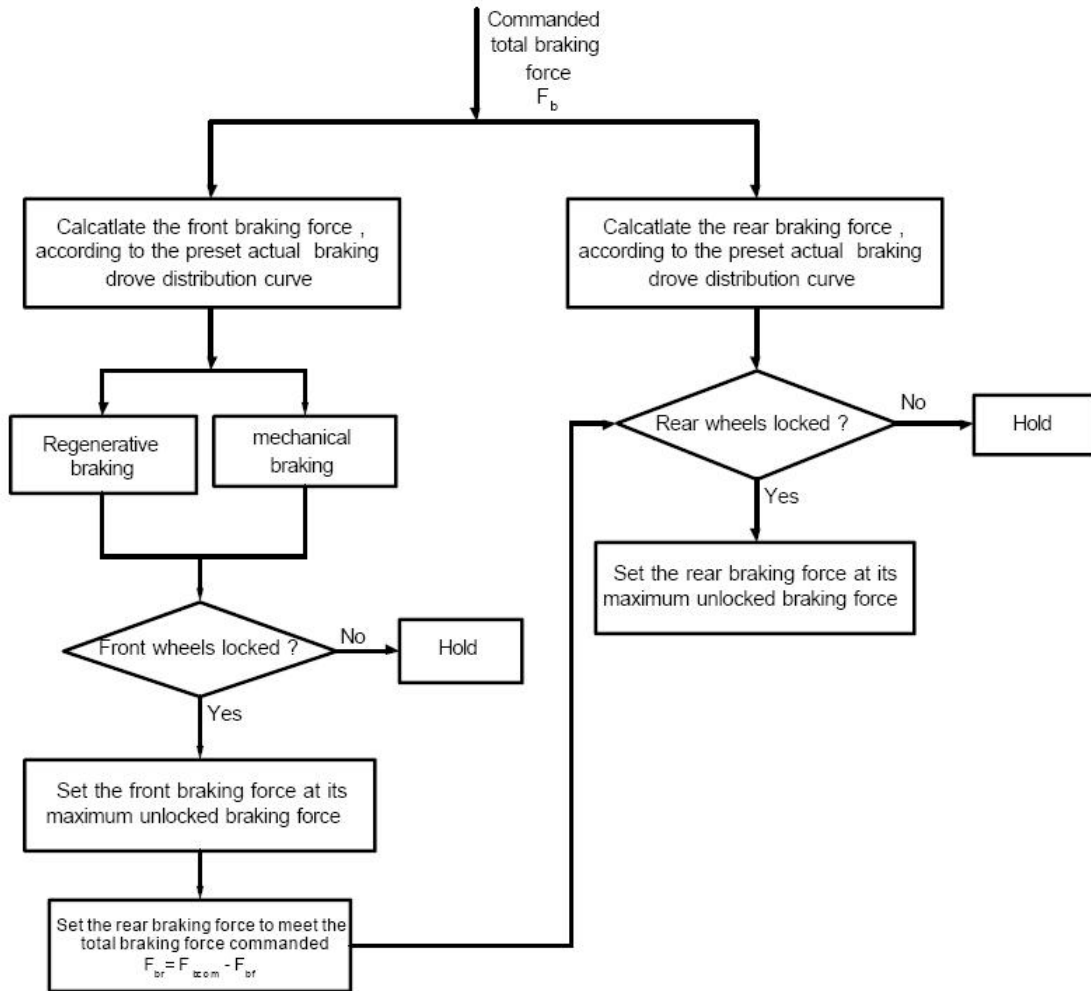


Figure 2-3. Control logic of brake forces of front and rear wheels [7]

(Reprinted with permission from SAE Paper 2001-01-2478 © 2001 SAE International)

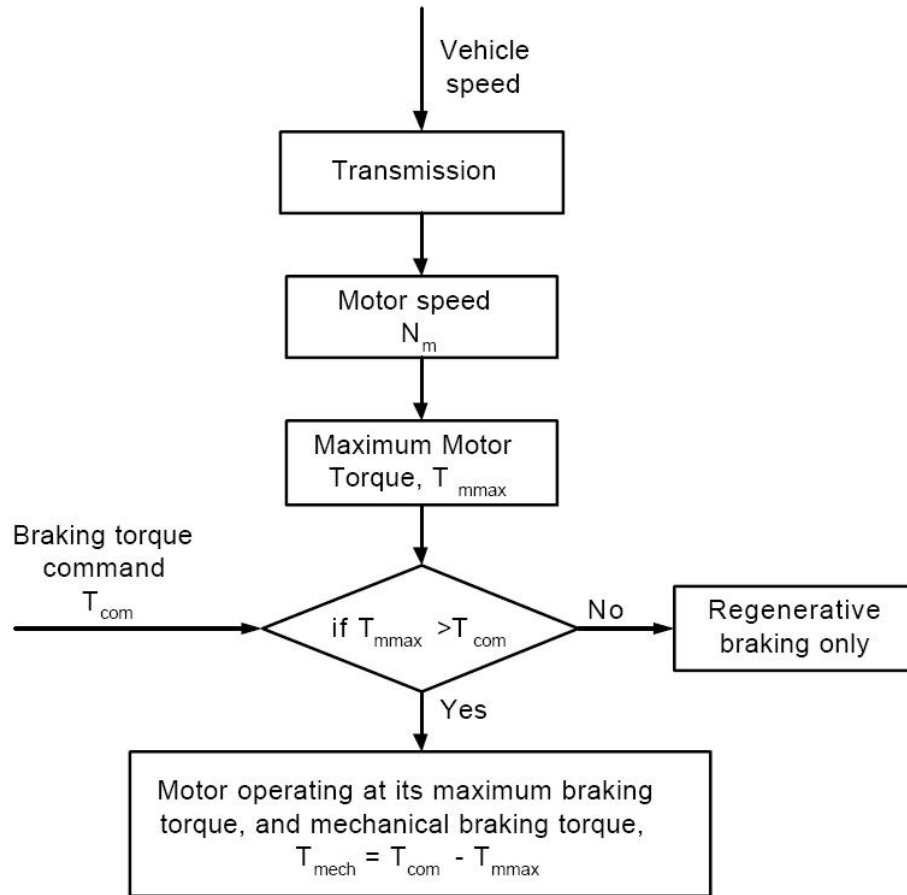


Figure 2-4. Control logic of brake force distribution to regenerative and mechanical brake systems [7]

(Reprinted with permission from SAE Paper 2001-01-2478 © 2001 SAE International)

Panagiotidis et al [8], develop a regenerative braking model for a parallel HEV including a wheel lock-up avoidance algorithm. They introduce a physics-based regenerative braking simulation for a diesel-assisted HEV in the MATLAB-SIMULINK-STATEFLOW and it is implemented in National Renewable Energy Laboratory's (NREL) HEV system simulation called ADVISOR. In this study, all braking events are categorized into four states and only one of them could be applied to braking events. The detailed states are described below from their paper.

STATE 1 – Neither the electric nor the hydraulic maximum brake forces can separately provide enough force to stop the vehicle.

STATE 2 – The amount of maximum front brake force is less than the wheel lock-up limit and also less than that which the generator is capable of providing.

STATE 3 – The required brake force for the front wheels reaches and/or exceeds a wheel lock-up scenario, either the generator alone supplies this force or the generator and frictional brakes supply the retarding force.

STATE 4 – The maximum brake force required at the wheels is greater than the lock-up force, but smaller than the maximum generator force available. This is called an “only-electric” mode.

Using the regenerative brake control strategy above, they simulate various vehicle configurations with different sizes of engine, motor and battery in the federal urban driving schedules (FUDS). The simulation results in 4 – 19% of improvement in fuel economy. The relatively large motor and battery have better fuel economy than the other configurations, because the larger motor could produce enough torque on demand during braking and the larger battery could have a larger capacity for recharging.

Duoba et al [9], estimate the regenerative brake system of a few HEVs on the current automotive market and investigate their fuel economy difference between in a single axle (2WD) and a double axle (4WD) dynamometer tests. They test a 2000 Honda Insight, a 2001 Toyota Prius, and a 2004 Toyota Prius with different drive cycles. According to their result, using a basic acceleration-deceleration cycle, the 2000 Honda Insight shows slightly lower fuel economy in the 4WD dynamometer test, but more energy is charged into the batteries than the 2WD dynamometer test result. It means that the overall fuel economy of both 2WD and 4WD dynamometer tests is almost equal. The other test result of the 2001 Toyota Prius using the NEDC and LA92 cycles shows slightly higher overall fuel economy on the 4WD dynamometer. In case of the 2004 Toyota Prius, the 4WD dynamometer test results in approximately 3% higher regenerative brake energy efficiency than 2WD dynamometer test result. In this study, the 2WD and 4WD dynamometer test results are described in Chapter 5 and they show slight difference but it is not very significant in terms of overall fuel economy.

In general, the regenerative brake system is not able to capture all brake energy, so there is a regenerative brake fraction, k . The value of k ($0 < k < 1$) can be determined by regenerative brake control strategies. In the simulation, a simple parallel regenerative brake control strategy in Figure 2-5 is used to simplify the model and see more direct impact of rotating inertia. At a given vehicle speed, frictional and regenerative brakes proportionally share the overall brake force by the value of k .

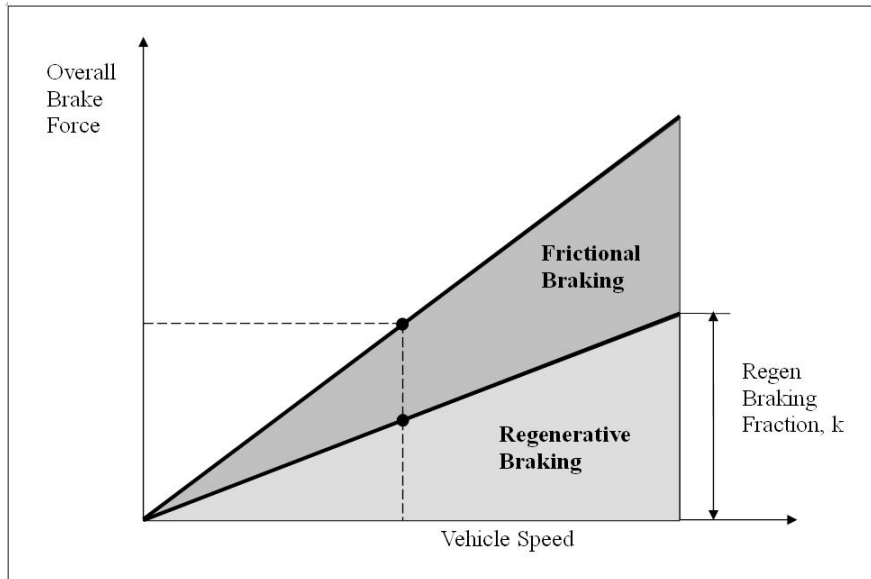


Figure 2-5. Series regenerative braking strategy

2.3 Motor Sizing for EV/HEV

In EVs, HEVs, and FCVs, the torque-speed characteristics of the electric traction motor are one of main factors which can affect the vehicle performance. A typical motor has two operational modes; the normal mode, or the constant torque region, and the extended mode, or the constant power region as shown in Figure 2-6.

Moore et al [10], estimate the vehicle acceleration performance with different ratios of the extended constant power range. In this study, they set up the ratio of the extended constant power region to the constant torque region range from 1:1 to 1:10. The acceleration times and distances, passing times and distances are calculated for each case. The results from this study show that the power requirement for acceleration is

decreased as the constant power region ratio is increased. However, the torque requirement for acceleration is increased as the constant power region ratio is increased. The last result shows that the passing performance is considerably decreased as the constant power region ratio is increased. Thus, determining the motor size is trade-off between motor characteristics and vehicle performance for different types of motor.

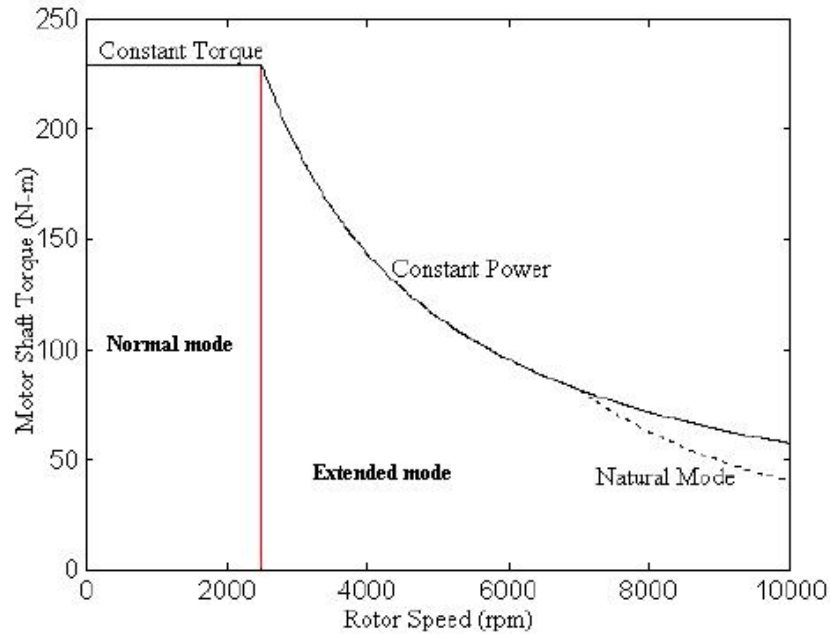


Figure 2-6. Typical motor characteristics [10]

(Reprinted with permission from SAE Paper 1999-01-1152 © 2001 SAE International)

Among various electric drive motor features such as torque density, inverter size, extended speed range-ability, energy efficiency, safety and reliability, and cost, the extended speed range-ability and energy efficiency are the two main characteristics for EVs, HEVs and FEVs. The vehicle acceleration performance is directly determined by the extended speed range-ability and the higher energy efficiency of the electric drive motor can improve the fuel economy of the vehicle. Rahman et al [11], investigate those two basic characteristics in a vehicular point of view using two software packages; V-ELPH developed by Texas A&M University and ADVISOR from NREL. A pure EV, series HEV, conventional vehicle, and parallel HEV are simulated with the FUDS and the federal highway driving schedules (FHDS) in this study. From their results, the

permanent magnet motor (PMM) is suitable for a strong HEV (50% hybridized) because it has superior energy efficiency in constant torque region. However, for a mild HEV (20% hybridized), the switched reluctance motor (SRM) could be a better choice since it has extended speed range-ability in constant power region compared to other motors.

Using the two software packages mentioned in the previous study, Rahman et al [12], research the effect of extended constant power operation of electric motor on a battery driven electric vehicle (BEV) or a pure EV. Five different vehicles are simulated with FUDS and HWFET cycles. Note that the HWFET cycle is the same as the FHDS. The results from the study show that the extended speed ratio of traction motors should be at least 1:3 to be able to meet the vehicle performance demand. If the ratio is below 1:3, then the EV should have larger battery cells due to poor performance, and it can increase the overall vehicle mass. However, beyond the extended speed ratio of 1:5 decreases the vehicle performance in terms of energy economy because high torque is required and it increases mass and volume of the motor. In addition, acceleration power does not decrease considerably beyond the ratio of 1:5 and it cannot reduce the battery size any more. Thus, the ratio beyond 1:5 increases the motor size and it increases the vehicle mass unnecessarily. According to their simulation results, the best extended speed ratio is 1:4 for a single gear EV propulsion system.

Chapter 3

Background Knowledge Applied to Simulation Model

Chapter 3 introduces the basic background knowledge applied to the simulation model. First, the vehicle forces are described with a schematic diagram and equations. The second section shows how the basic idea of a rotating inertia is applied to the simulation model for analysis. Also it explains what kind of rotating components are in a vehicle and which ones are selected as dominant rotating components for this study.

3.1 Vehicle Forces

As mentioned in Chapter 2, the fundamental knowledge about vehicle performance analysis is well described in many text books [2, 3, 4]. In this section, forces acting on a vehicle in the direction of acceleration are defined and each term is explained briefly.

3.1.1 Tractive Force and Acceleration

In order to propel a vehicle, the vehicle should overcome certain resistance forces such as aerodynamic drag resistance, rolling resistance, grading resistance, towing resistance, and inertial forces. Figure 3-1 shows those resistance forces schematically. Each term in Figure 3-1 is described in equations below.

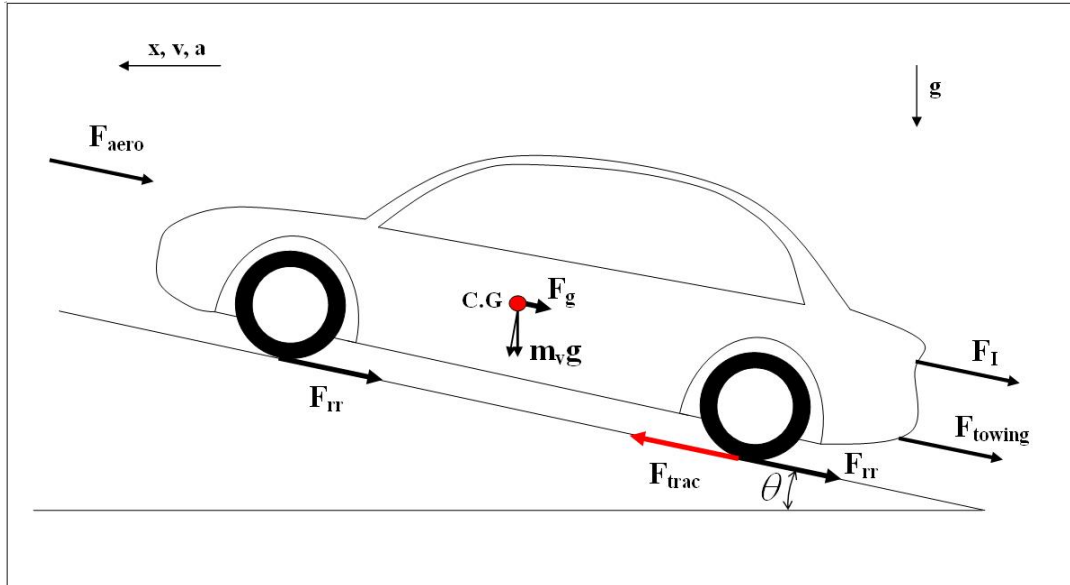


Figure 3-1. Diagram of forces acting on a vehicle

Equation (3-1) represents the aerodynamic drag resistance which is proportional to the air drag coefficient, the frontal area of the vehicle and the square of the vehicle speed as well. A larger frontal area and higher vehicle speed increase the aerodynamic drag resistance.

$$F_{aero} = \frac{1}{2} \rho C_D A V^2 \quad (3-1)$$

- where: ρ = Density of air (kg/m^3)
 C_D = Air drag coefficient
 A = Frontal area of a vehicle (m^2)
 V = Vehicle speed (m/s)

The rolling resistance can be expressed as equation (3-2). The rolling resistance on front and rear wheels could be varied depending on the mass distribution of the vehicle and the size or type of tires. However, if the rolling resistance coefficients of front and rear wheels are set up to be same, then it is not necessary to consider the mass distribution of the vehicle for the overall rolling resistance.

$$F_{rr} = [C_{rr,front} m_f + C_{rr,rear} (1 - m_f)] m_v g \cos \theta \quad (3-2)$$

where: $C_{rr,front}$ = Rolling resistance coefficient of front wheels

$C_{rr,rear}$ = Rolling resistance coefficient of rear wheels

m_f = Fraction of mass on front axle

m_v = Total mass of test vehicle (kg)

g = Acceleration of gravity (m/s^2)

θ = Angle of the road from horizontal (rad)

Equation (3-3) is the grade force due to the angle of the road.

$$F_g = m_v g \sin \theta \quad (3-3)$$

For the towing force in Figure 3-1, an additional mass could be simply added to the test vehicle mass assuming that a trailer has negligible impact on drag forces. In general, the equation of motion of a vehicle along the x-axis (longitudinal direction) is given by

$$m_{eff} a_x = F_{trac} - F_{aero} - F_{rr} - F_g - F_{tow} \quad (3-4)$$

where: m_{eff} = Effective mass of a vehicle (kg)

a_x = Longitudinal acceleration (m/s^2)

F_{trac} = Tractive force at the ground (N)

F_{rr} = Rolling resistance force of all wheels (N)

F_{aero} = Aerodynamic drag force (N)

F_{tow} = Towing force (N)

F_g = Resistance force by grade (N)

In other words, equation (3-4) could be rearranged in terms of the tractive force which can propel the vehicle.

$$F_{trac} = F_{aero} + F_{rr} + F_g + F_{tow} + m_{eff}a_x \quad (3-5)$$

In this equation, the inertial force term with the effective mass, $m_{eff}a_x$, represents all inertial forces which include translational inertial force and all rotating inertial forces.

In a conventional vehicle, there are many rotating components such as a crank shaft, pulleys, axles, wheels and tires, and so on. All rotating components in a vehicle have rotating inertias, and have an effect on vehicle performance analysis. However small rotating components such as pulleys and bearings have relatively small contributions on the vehicle performance analysis compared to larger rotating components [3]. Therefore, three main components such as motor/generator, driveline, and wheel/tire assemblies are selected to simplify the simulation in this analysis. Thus, using those main rotating components, the effective mass of a vehicle could be obtained by the equation below.

$$m_{eff} = m_v + 4 \frac{I_{w/t}}{r_r^2} + \frac{I_{driveline} N_t^2 N_f^2}{r_r^2} + \frac{I_{M/G} N_t^2 N_f^2}{r_r^2} \quad (3-6)$$

where: m_v = Total mass of test vehicle (kg)

$I_{w/t}$ = Moment of inertia of each wheel/tire assembly(kg-m²)

$I_{driveline}$ = Moment of inertia of driveline (kg-m²)

$I_{M/G}$ = Moment of inertia of a motor/generator (kg-m²)

N_t = Transmission gear ratio

N_f = Final drive gear ratio

r_r = Rolling radius of a wheel (m)

The second term on the right hand side represents the rotating inertial mass of four wheels and tires. The other terms represent the rotating inertial mass of the driveline and the motor/generator. Figure 3-2 describes the schematic diagram of a vehicle with ratios and rotating inertia at each component which are used in equation (3-6).

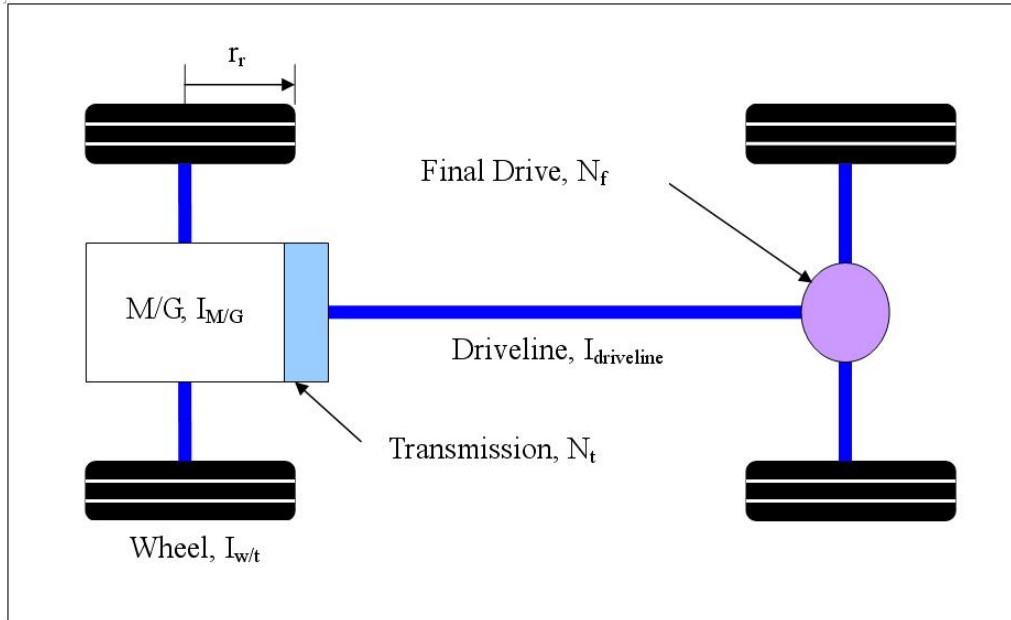


Figure 3-2. Schematic diagram of a vehicle with ratios and rotating inertia at each component

Multiplying equation (3-6) by the acceleration gives the inertial force acting on a vehicle. In equation (3-7), each term on the right hand side is related to the vehicle speed by the rolling radius, the transmission gear and final drive gear ratios, so that the acceleration of the vehicle, a_x , can be used.

$$m_{eff} a_x = \left(m + 4 \frac{I_{w/t}}{r_r^2} + \frac{I_{driveline} N_t^2 N_f^2}{r_r^2} + \frac{I_{M/G} N_t^2 N_f^2}{r_r^2} \right) a_x \quad (3-7)$$

$$F_I = F_{trans,I} + F_{w/t,I} + F_{driveline,I} + F_{M/G,I}$$

Obviously, if a vehicle has zero acceleration, then the inertial force is zero. More details about inertial mass and force are described in next section.

3.1.2 Inertial Forces

Let's consider each inertial force term separately. The first term on the right hand side of equation (3-7) is the translational inertial force, $F_{I,translation}$, which can be simply expressed as multiplication of the test vehicle mass and the acceleration.

$$F_{I,translation} = m_v a_x \quad (3-8)$$

where: $F_{I,translation}$ = Translational inertial force (N)

In general, a so-called wheel is an assembly of a wheel and a tire and they have different mass and different size. Therefore, the moment of inertia for both components is considered separately. Also, it is assumed that a wheel and a tire have the same center of mass at a rotating axis and the mass is symmetrically distributed on their outer diameters. From these assumptions, the moment of inertia of a thin ring-shaped object, as shown in Figure 3-3, is simply used to determine the second term of equation (3-7) which is the rotating inertial force of wheels and tires.

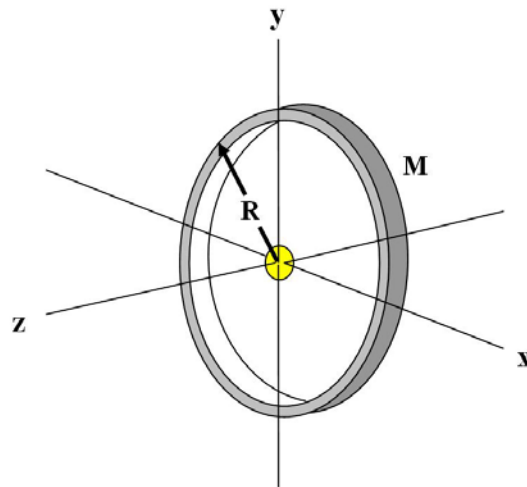


Figure 3-3. Moment of inertia for a thin ring shape object

If M is the mass and R is the radius, then the moment of inertia of a thin ring shape object is given by:

$$I = MR^2 \quad (3-9)$$

where: I = Moment of inertia (kg-m²)
 M = Mass of a ring shape object (kg)
 R = Radius of a ring shape object (m)

Thus, the moment of inertia of a wheel/tire assembly can be defined as shown below.

$$I_{w/t} = m_w r_w^2 + m_t r_t^2 \quad (3-10)$$

where: $I_{w/t}$ = Moment of inertia of each wheel/tire assembly (kg-m²)
 m_w = Mass of a wheel (kg)
 r_w = Outer radius of a wheel (m)
 m_t = Mass of a tire (kg)
 r_t = Outer radius of a tire (m)

From equations (3-7) & (3-10), the rotating inertial force for four wheel and tire assemblies can be obtained.

$$F_{I,t/w} = 4 \frac{I_{w/t}}{r_r^2} a_x \quad (3-11)$$

where: $F_{I,t/w}$ = Rotating inertial force of four wheel/tire assemblies (N)

The moment of inertia for the driveline and motor (M/G) is slightly different from that of a wheel and tire assembly. Equation (3-12) which is a moment of inertia for a cylindrical object can be applied for the driveline and the M/G.

$$I = \frac{1}{2}MR^2 \quad (3-12)$$

However, the values of moment of inertia for the driveline and motor (M/G) are obtained from measured or calculated data in this analysis, due to lack of accurate values for calculation.

3.2 Basic Idea of Rotating Inertia

Figure 3-4 shows the basic idea of rotating inertia which is applied to the simulation model in this study. In general, power is transmitted from the input shaft to the output shaft through the cylindrical object while it is being accelerated. In this case, the output power is generally less than the input power except that there is no translating acceleration, because it has its own rotating inertia. Due to this rotating inertia, certain amount of power can be stored to the rotating object and the rest of power comes out through the output shaft. On the other hand, the stored power can be discharged in deceleration and it can be captured and stored to a storage system. Note that, in deceleration, the direction of angular acceleration becomes opposite to acceleration, but the direction of rotation can be either same or opposite.

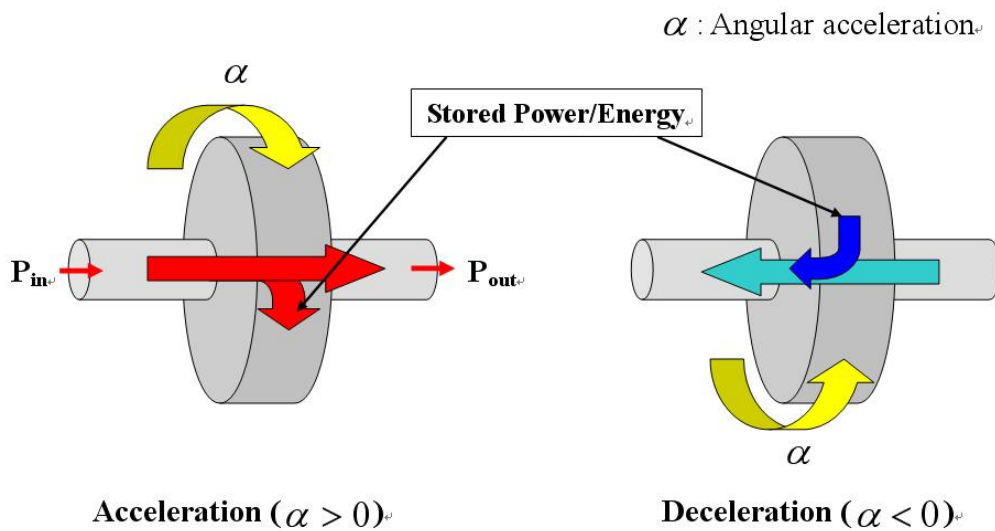


Figure 3-4. Basic concept of charging and discharging of rotating inertial power/energy

If the power is integrated over time, then it becomes energy. In this study, the simple basic idea of charging and discharging power or energy of a rotating object is used to estimate individual contribution of rotating components in terms of energy recovery over various drive cycles.

Chapter 4

Simulation Model

In Chapter 4, a more detailed explanation about the simulation model is presented. Using equations and ideas from Chapter 3, power and energy equations are derived for propulsion and braking cases. In the derivation of the equations, slightly different approach is applied rather than the equations using the effective mass in Chapter 3. Determination of motor/generator efficiency, acceleration performance, and trace miss analyses are covered in later sections of this Chapter 4.

4.1 Tractive Power

Equation (3-5) in Chapter 3 shows the tractive force which can propel the vehicle with the effective mass. Substituting the inertial force, equation (3-7), into the tractive force, equation (3-5), then it gives more detailed expression for the tractive force.

$$F_{trac} = F_{aero} + F_{rr} + \left(m_v + 4 \frac{I_{w/t}}{r_r^2} + \frac{I_{driveline} N_t^2 N_f^2}{r_r^2} + \frac{I_{M/G} N_t^2 N_f^2}{r_r^2} \right) a_x \quad (4-1)$$

Note that the there is no grade resistance and no towing forces in this study, so the tractive force is reduced as shown in equation (4-1). Multiplying the tractive force by the velocity of the vehicle gives the total tractive power required to accelerate or decelerate the whole vehicle (equation (4-2)) including all rotating components such as wheel/tire assemblies, driveline, M/G and so on.

$$P_{trac} = F_{trac} V$$

or

(4-2)

$$P_{trac} = V \left(F_{aero} + F_{rr} + \left(m_v + 4 \frac{I_{w/t}}{r_r^2} + \frac{I_{drive\ line} N_t^2 N_f^2}{r_r^2} + \frac{I_{M/G} N_t^2 N_f^2}{r_r^2} \right) a_x \right)$$

where: P_{trac} = Total tractive power required to propel a vehicle (W)

V = Velocity of the vehicle

In general, if a driver hits a gas pedal on a vehicle, an engine or a motor generates power to propel the vehicle, then the vehicle is being accelerated on a flat road. Also, if he or she releases it, then the vehicle is being decelerated due to resistance forces. However, if the road is uphill and a vehicle can not provide enough power to overcome resistance forces, then the vehicle could be in deceleration. In this case, it can not be directly determined whether the vehicle is in acceleration or deceleration by generating power from power source. Therefore, P_{trac} is used to determine the state of a vehicle in the simulation model. For example, if P_{trac} is positive, then the vehicle is in acceleration and if P_{trac} is negative, then the vehicle is in deceleration. Obviously, if P_{trac} is zero, then the vehicle is either stopped or coasting.

4.2 Propulsion

4.2.1 Power and Energy Required to Propel

The total tractive power, P_{trac} , is slightly different from the actual tractive power required to propel a vehicle from a power source. Tracking backward from the ground to the power source and considering efficiency of each component give the expression for it. First, at the contact point between four wheels and the ground, the vehicle needs certain amount of power to overcome the resistance forces and the translational force for propulsion and this is the power output from driven wheels, $P_{w/t,out}$.

$$P_{w/t,out} = V \{ F_{aero} + F_{rr} + m_v a_x \} \quad (4-3)$$

where: $P_{w/t,out}$ = Power output from driven wheels to the ground (W)

Figures 4-1, 4-2 and 4-3 show the power flow schematic configurations of power flow of propelling for AWD, FWD, and RWD vehicles respectively. In the figures below, each drive type shows slightly different power flow from the driveline to the wheels, however, calculations are all same for each case. Because even the output power from the driveline is separated to the front and rear wheel in AWD case, but the summation of the output power at each wheel gives the same overall output power as the FWD and RWD cases.

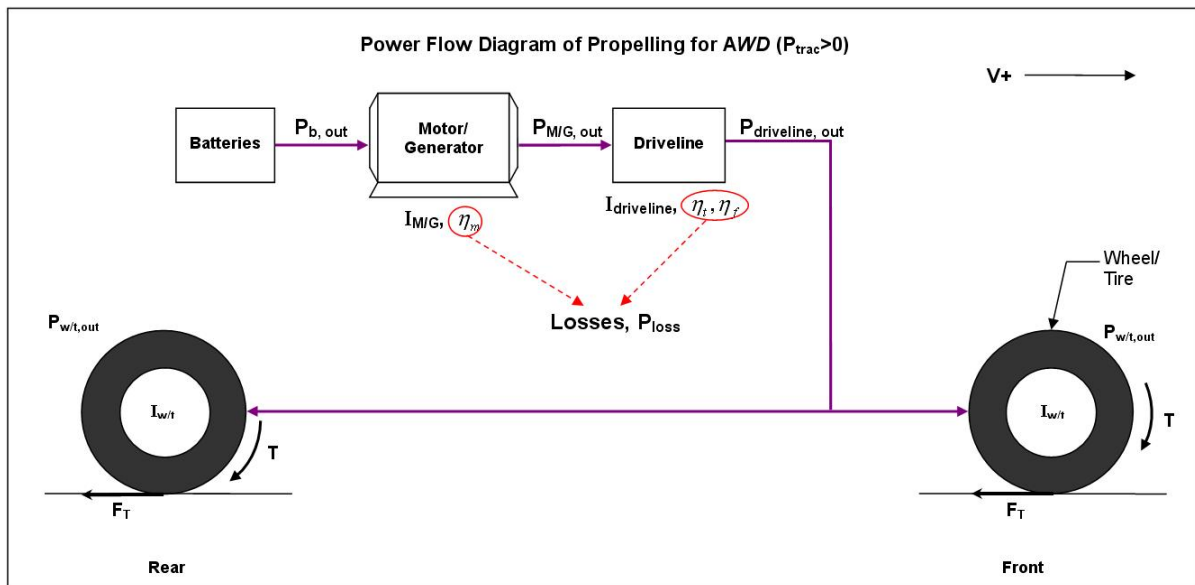


Figure 4-1. Power flow diagram of propelling for AWD vehicle

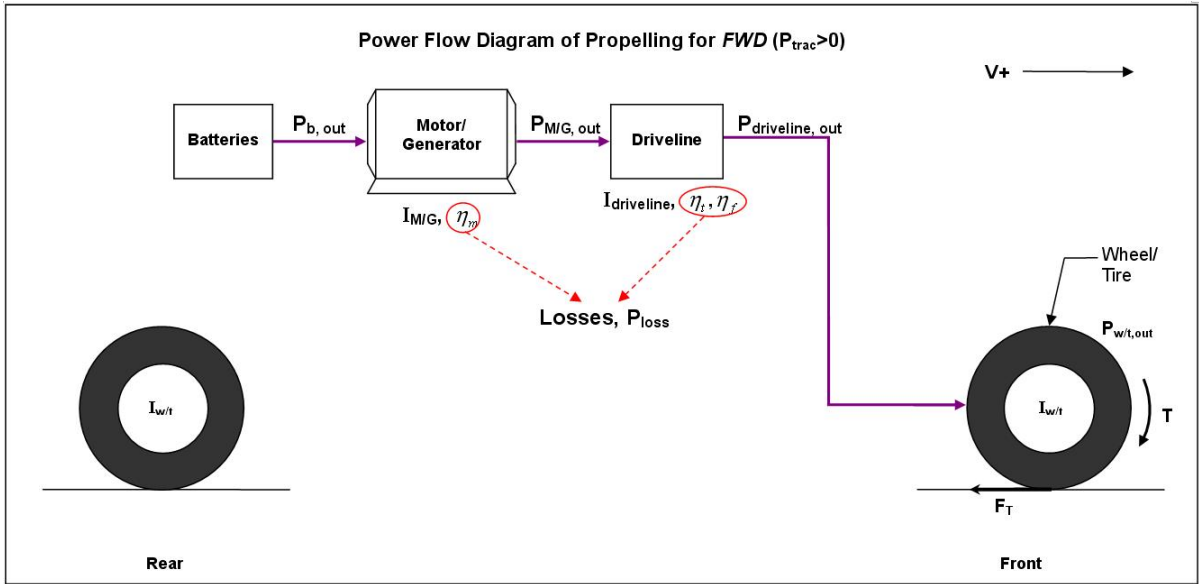


Figure 4-2. Power flow diagram of propelling for FWD vehicle

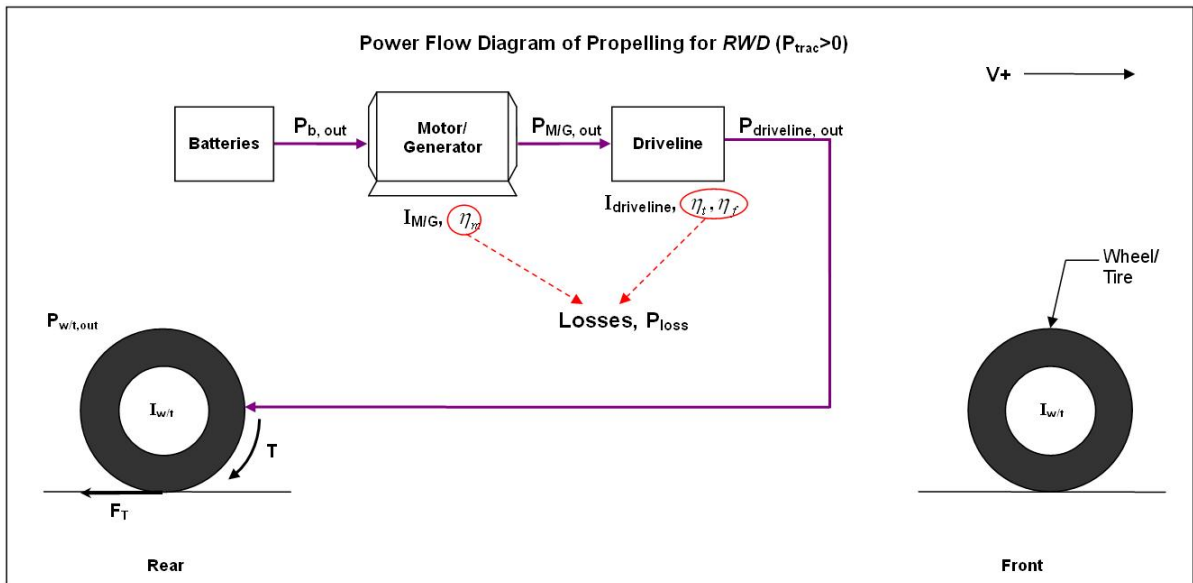


Figure 4-3. Power flow diagram of propelling for RWD vehicle

In order to propel the vehicle and driven wheels, it needs more power to overcome the rotating inertial force of wheel/tire assemblies. Thus the rotating inertial power of wheel/tire assemblies could be added to the actual tractive power. Equation (4-4) below shows the power output from driveline.

$$P_{driveline,out} = V \left\{ F_{aero} + F_{rr} + \left(m_v + 4 \frac{I_{w/t}}{r_r^2} + \right) a_x \right\} \quad (4-4)$$

where: $P_{driveline,out}$ = Power output from driveline to propel a vehicle (W)

The driveline loses certain amount of power by friction between each component such as bearings and gears. Also, the actual tractive power from the power source accelerates the driveline to propel the vehicle. Thus the rotating inertial power of driveline should be considered. Equation (4-5) shows the power output from the M/G which includes the efficiencies of the transmission and the final drive, and the rotating inertial power.

$$P_{M/G,out} = \frac{V}{\eta_t \eta_f} \left[\left\{ F_{aero} + F_{rr} + \left(m_v + 4 \frac{I_{w/t}}{r_r^2} + \right) a_x \right\} + \frac{I_{driveline} N_t^2 N_f^2}{r_r^2} a_x \right] \quad (4-5)$$

where: $P_{M/G,out}$ = Power output from M/G to propel a vehicle (W)

The M/G has efficiency along with the torque and the speed, thus it also loses certain amount of power. Again, the actual power from the power source uses some portion of it to accelerate the M/G. Finally, considering efficiency and the rotating inertial power of the M/G yields the actual tractive power required to propel the whole vehicle including rotating components.

$$P_{b,out} = \frac{V}{\eta_{M/G}} \left[\frac{1}{\eta_t \eta_f} \left[\left\{ F_{aero} + F_{rr} + \left(m_v + 4 \frac{I_{w/t}}{r_r^2} + \right) a_x \right\} + \frac{I_{driveline} N_t^2 N_f^2}{r_r^2} a_x \right] + \frac{I_{M/G} N_t^2 N_f^2}{r_r^2} a_x \right] \quad (4-6)$$

where: $P_{b,out}$ = Power output from a battery to propel a vehicle (W)

From the $P_{b,out}$, the energy output from the battery, $E_{b,out}$, can be obtained by integrating $P_{b,out}$ over the time.

$$E_{b,out} = \int_{Propulsion} P_{b,out} dt$$

where: $E_{b,out}$ = Energy output from a battery during propulsion (J)

4.2.2 Power Losses during Propulsion

Again, as shown in Figures 4-1, 4-2 and 4-3, there are power losses because of M/G and driveline inefficiencies. Equations (4-7), and (4-8) show the power losses at driveline and M/G respectively.

$$P_{driveline,loss} = (1 - \eta_t \eta_f) \frac{V}{\eta_t \eta_f} \left[\left\{ F_{aero} + F_{rr} + \left(m_v + 4 \frac{I_{w/t}}{r_r^2} + \right) a_x \right\} + \frac{I_{driveline} N_t^2 N_f^2}{r_r^2} a_x \right] \quad (4-7)$$

$$P_{M/G,loss} = (1 - \eta_{M/G}) \frac{V}{\eta_{M/G}} \left[\frac{1}{\eta_t \eta_f} \left[\left\{ F_{aero} + F_{rr} + \left(m_v + 4 \frac{I_{w/t}}{r_r^2} + \right) a_x \right\} + \frac{I_{driveline} N_t^2 N_f^2}{r_r^2} a_x \right] + \frac{I_{M/G} N_t^2 N_f^2}{r_r^2} a_x \right] \quad (4-8)$$

4.2.3 Difference between on-road and dynamometer tests

The equations above are for a real-driving test (on-road test) with all wheels spinning. However, there is a small difference between the on-road and the dynamometer tests. In case of the dynamometer test, only one axle (two wheels) is

rotating in a single roll dynamometer, so the rotating inertial power should be reduced down to half of the on-road test case. It is shown below.

$$P_{w/t,inertia} = 2 \frac{I_{w/t}}{r^2} a_x V \quad (4-9)$$

where: $P_{w/t,inertia}$ = Rotating inertial power of two wheel/tire assemblies (W)

4.3 Braking (Regenerative Braking)

4.3.1 Regenerative Brake Power and Energy

In order to capture the regenerative brake power/energy, the value of P_{trac} should be always negative. For example, if the tractive power from the M/G is less than the road load (loss) but not zero, then the vehicle is being decelerated because there is not enough tractive power to accelerate the vehicle. In this situation, the regenerative brake system cannot capture the regenerative brake power/energy since the P_{trac} is still positive. It means that the M/G and driveline are still being operated to propel the vehicle as it decelerates.

Thus, when the value of P_{trac} is negative, the power input into the battery, which is available to be captured from the regenerative braking, can be calculated. Multiplying it by a regenerative brake ratio and final drive, the transmission, and motor efficiencies for each term yields the power input into the battery. Figures 4-4, 4-5, and 4-6 show the schematic configurations of power flow of regenerative braking for AWD, FWD, and RWD cases respectively.

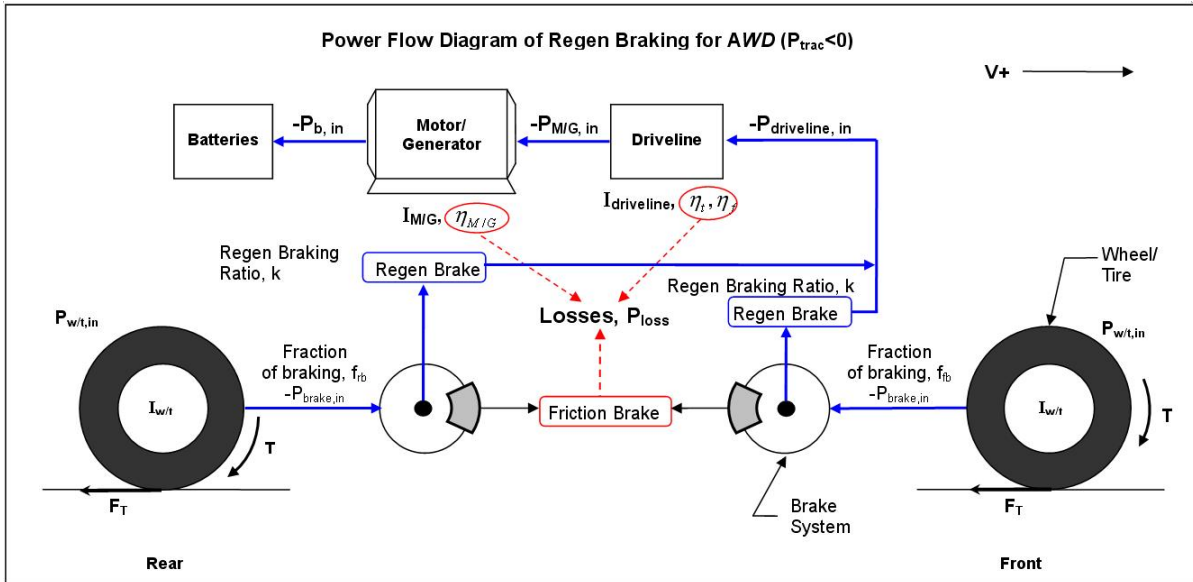


Figure 4-4. Power flow diagram of regenerative braking for AWD vehicle during braking

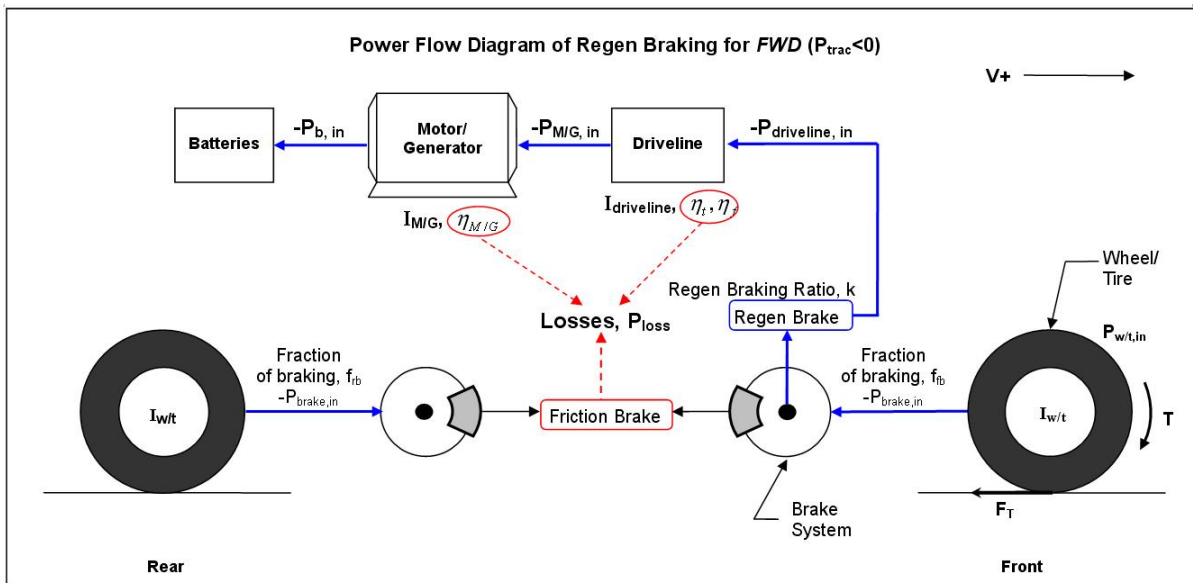


Figure 4-5. Power flow diagram of regenerative braking for FWD vehicle during braking

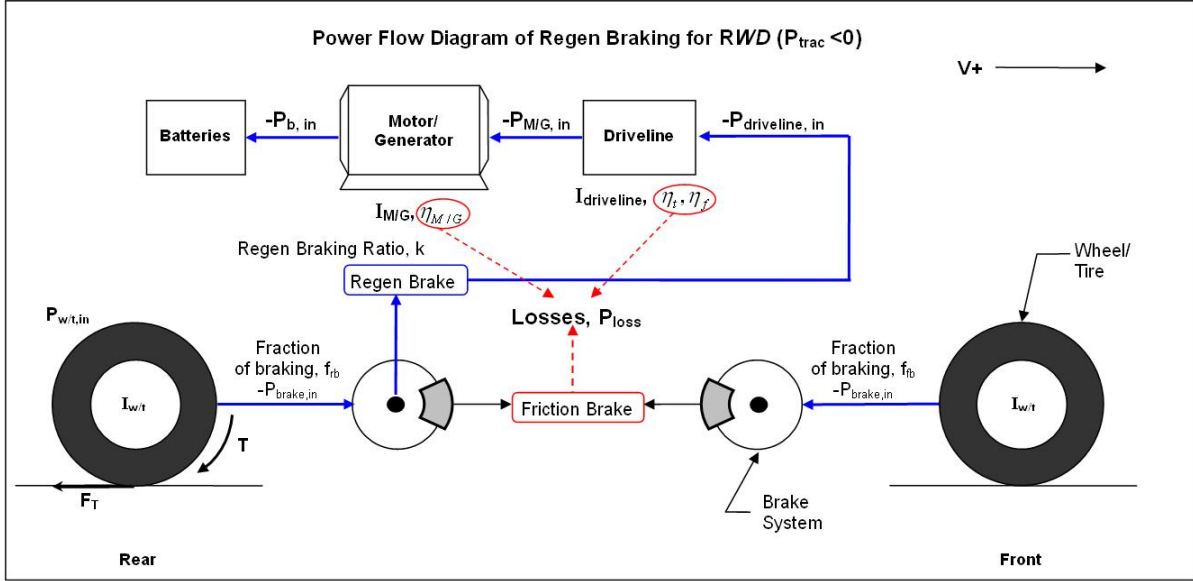


Figure 4-6. Power flow diagram of regenerative braking for RWD vehicle during braking

The following steps show more details. First, the summation of resistance forces, and the translational inertial force gives the power input into the wheel/tire assemblies at ground, $P_{w/t, in}$, by braking.

$$P_{w/t, in} = V \{ F_{aero} + F_{rr} + m_v a_x \} \quad (4-10)$$

where: $P_{w/t, in}$ = Power input at ground by braking (W)

V = Velocity of the vehicle

Then, adding up the rotating inertial power of four wheel/tire assemblies to the $P_{w/t, in}$ gives the brake power required at the driven wheels during braking. In general, the fraction of front braking, f_{fb} , is larger than that of rear braking, f_{rb} , since the rear brake should avoid locking of rear wheels at maximum braking. Therefore, the value of fraction, f_b ($0 < f_b \leq 1$), should be multiplied to the $P_{w/t, in}$. If a vehicle is AWD, then the fraction of braking could be 1, because two axles (four wheels) are able to capture regenerative brake power/energy. However, in case of a FWD or a RWD vehicle, only one axle (two wheels) is able to capture regenerative brake power/energy. Thus

the f_b becomes less than 1. Equation (4-11) shows the $P_{brake, in}$.

$$P_{brake, in} = f_b V \left\{ F_{aero} + F_{rr} + \left(m_v + 4 \frac{I_{w/t}}{r_r^2} \right) a_x \right\} \quad (4-11)$$

where: $P_{brake, in}$ = Power input into brake system by braking (W)

f_b = Fraction of braking at driven axle ($0 < f_b \leq 1$)

$$\begin{cases} AWD: f_b = 1 \\ FWD: f_b = f_{fb} \\ RWD: f_b = 1 - f_{fb} \end{cases}$$

f_{fb} = Fraction of front braking ($0 < f_{fb} < 1$)

f_{rb} = Fraction of rear braking ($0 < f_{rb} < 1$)

Multiplying the regenerative brake fraction, k , into the $P_{brake, in}$ yields the power input into the driveline by regenerative braking. The $P_{driveline, in}$ is shown below in equation (4-12).

$$P_{driveline, in} = k f_b V \left\{ F_{aero} + F_{rr} + \left(m_v + 4 \frac{I_{w/t}}{r_r^2} \right) a_x \right\} \quad (4-12)$$

where: $P_{driveline, in}$ = Power input into driveline by regenerative braking (W)

k = Regenerative brake fraction

Applying final drive and transmission efficiencies and adding the rotating inertial power of driveline gives the power input into the M/G which can be captured from the driven axles.

$$P_{M/G,in} = \eta_t \eta_f V \left[kf_b \left\{ F_{aero} + F_{rr} + \left(m_v + 4 \frac{I_{w/t}}{r_r^2} \right) a_x \right\} + \frac{I_{driveline} N_t^2 N_f^2}{r_r^2} a_x \right] \quad (4-13)$$

where: $P_{M/G,in}$ = Power input into M/G by regenerative braking (W)

η_t = Transmission efficiency

η_f = Final drive efficiency

Then, the M/G inertial power can be added to the power input into the battery. Finally, adding up all together gives the power input into the battery by regenerative braking, $P_{b,in}$, only if the P_{trac} is negative.

$$P_{b,in} = \eta_{M/G} V \left[\eta_t \eta_f \left[kf_b \left\{ F_{aero} + F_{rr} + \left(m_v + 4 \frac{I_{w/t}}{r_r^2} \right) a_x \right\} + \frac{I_{driveline} N_t^2 N_f^2}{r_r^2} a_x \right] + \frac{I_{M/G} N_t^2 N_f^2}{r_r^2} a_x \right] \quad (4-14)$$

where: $P_{b,in}$ = Power input into a battery by regenerative braking (W)

$\eta_{M/G}$ = M/G efficiency

Again, from the $P_{b,in}$, the energy input into the battery, $E_{b,in}$, can be obtained by integrating $P_{b,in}$ over the time.

$$E_{b,in} = \int_{braking} P_{b,in} dt \quad (4-15)$$

where: $E_{b,in}$ = Energy input into a battery by regenerative braking (J)

4.3.2 Power Losses during Regenerative Braking

The power losses during regenerative braking can be simply calculated. They occur because of M/G, transmission, and final drive efficiencies. Equations (4-16), (4-17), (4-18), and (4-19) show the power losses at un-driven axle, friction braking, driveline, and M/G. respectively.

$$P_{undriven\ axle,loss} = (1 - f_b)V \left\{ F_{aero} + F_{rr} + \left(m_v + 4 \frac{I_{w/t}}{r_r^2} \right) a_x \right\} \quad (4-16)$$

In case of an AWD vehicle, the value of $P_{undriven\ axle,loss}$ becomes zero since the fraction of braking, f_b , is 1. However, for a FWD or RWD vehicle, the power loss at un-driven axle is not zero.

$$P_{brake,loss} = (1 - k)f_b V \left\{ F_{aero} + F_{rr} + \left(m_v + 4 \frac{I_{w/t}}{r_r^2} \right) a_x \right\} \quad (4-17)$$

$$P_{driveline,loss} = (1 - \eta_t \eta_f)V \left[kf_b \left\{ F_{aero} + F_{rr} + \left(m_v + 4 \frac{I_{w/t}}{r_r^2} \right) a_x \right\} + \frac{I_{driveline} N_t^2 N_f^2}{r_r^2} \right] \quad (4-18)$$

$$P_{M/G,in} = (1 - \eta_{M/G}) \eta_t \eta_f V \left[\left[kf_b \left\{ F_{aero} + F_{rr} + \left(m_v + 4 \frac{I_{w/t}}{r_r^2} \right) a_x \right\} + \frac{I_{driveline} N_t^2 N_f^2}{r_r^2} a_x \right] \frac{I_{M/G} N_t^2 N_f^2}{r_r^2} a_x \right] \quad (4-19)$$

4.4 Determination of Motor/Generator Efficiency

In the power equations of both regenerative braking and propulsion cases, there is a M/G efficiency, $\eta_{M/G}$. The value of $\eta_{M/G}$ can be calculated from the torque and the M/G speed at the output shaft. The M/G speed can be calculated using equation (4-22).

$$S_{M/G} = \frac{60}{2\pi} \frac{N_r N_f}{r_r} V \quad (4-22)$$

where: $S_{M/G}$ = M/G speed at output shaft (rpm)

Also the torque at M/G shaft can be calculated from the equation (4-23)

$$T_{M/G} = \frac{P_{M/G}}{\omega_{M/G}} \quad (4-23)$$

where: $T_{M/G}$ = Torque of M/G at output shaft (N-m)

$P_{M/G}$ = Power of M/G at output shaft (W) ($P_{M/G,in}$ or $P_{M/G,out}$)

$\omega_{M/G}$ = Angular velocity of M/G at output shaft (rad/s)

The power of M/G at output shaft, $P_{M/G}$, could be either $P_{M/G,in}$ or $P_{M/G,out}$ depending on regenerative braking or propulsion case. The angular velocity of M/G at output shaft, $\omega_{M/G}$, could be converted from the $S_{M/G}$.

$$\omega_{M/G} = S_{M/G} \frac{2\pi}{60} \quad (4-24)$$

In order to obtain a M/G efficiency at a given vehicle velocity, the data of Table A-1 in Appendix A is used. If the efficiency value which is not shown on Table A-1 can be calculated by interpolating the values of torque and M/G speed. Note that efficiency is assumed to be symmetric for positive or negative torque.

4.5 Acceleration Performance Analysis

In this study, the acceleration performance analysis is simulated such as top speed and 0-60 mph time to determine a motor size. For a given vehicle speed, V , the acceleration of the vehicle can be calculated by using the following calculation procedure [13]. First, the overall gear ratio can be simply calculated from equation (4-25).

$$G = \frac{2\pi}{60} \frac{r_r}{N_t N_f} (m/s \cdot rpm) \quad (4-25)$$

where: G = Overall gear ratio

This overall gear ratio relates the vehicle speed to the motor speed. Using the overall gear ratio, G , the motor speed can be determined as shown below.

$$S_{M/G} = \frac{V}{G} (rpm) \quad (4-26)$$

Before the next step, the motor speed should be checked whether it exceeds the maximum motor speed or not. If it does, the motor speed is limited by the maximum motor speed at the given vehicle speed. The tractive force for acceleration performance analysis can be obtained with motor speed and torque.

$$F_t = T_{M/G} \frac{N_t N_f}{r_r} \eta_t \eta_f \quad (4-27)$$

where: F_t = Tractive force for acceleration performance analysis (N)

Also, the drag forces (resistance forces) can be easily calculated by equation (4-28).

$$F_d = F_{aero} + F_{rr} + F_g + F_{tow} \quad (4-28)$$

In this analysis, it is assumed that there are no grade resistance and no towing forces, so equation (4-28) can be reduced to $F_d = F_{aero} + F_{rr}$. Subtracting the drag force from the tractive force gives the propulsive force shown below.

$$F_p = F_t - F_d \quad (4-29)$$

where: F_p = Propulsive force (N)

If the propulsive force is divided by the effective mass, m_{eff} , which is shown in equation (3-6), then it becomes the longitudinal acceleration of the vehicle.

$$a_x = \frac{F_p}{m_{eff}} \quad (4-30)$$

Using the acceleration, cumulative time and distance can be estimated with equations (4-31) and (4-32).

$$t_i = t_{i-1} + \Delta t = t_{i-1} + \left[\frac{\frac{1}{a_{i-1}} + \frac{1}{a_i}}{2} \right] \Delta V \quad (4-31)$$

where: t_i = Cumulative time at i^{th} step

t_{i-1} = Cumulative time at $i-1^{\text{th}}$ step

Δt = Incremental time

a_i = Acceleration at i^{th} step

a_{i-1} = Acceleration at $i-1^{\text{th}}$ step

ΔV = Incremental speed of the vehicle

$$s_i = s_{i-1} + \Delta s = s_{i-1} + \left(V_{i-1} + \frac{\Delta V}{2} \right) \Delta t \quad (4-32)$$

where: s_i =Cumulative distance at i^{th} step

s_{i-1} =Cumulative distance at $i-1^{\text{th}}$ step

Δs = Incremental distance traveled by the vehicle

V_{i-1} = Vehicle speed at $i-1^{\text{th}}$ step

Also, if the acceleration in equation (4-30) becomes negative, it means that the vehicle cannot generate enough power to accelerate and the vehicle speed at this point could be top speed.

The specifications of the vehicle used in this analysis are described in Tables 4-2 and 4-3 in section 4.7. Using those vehicle specifications, the acceleration performance test is simulated. In fact, the motor parameters in Table 4-3 and the gearing are primarily sized to meet the vehicle performance goals of: 0-60 mph time less than 10 seconds, greater than 100 mph of top speed, and less than 2 mph trace miss on the US06 drive cycle. The result of the vehicle acceleration performance is tabulated in Table 4-1 and it gives results for drive cycles in Chapter 5.

Table 4-1. Vehicle acceleration performance

0-60 mph time	(sec)	9.45
Top speed	(mph)	105
US06 drive cycle trace miss	(<mph)	2 mph

4.6 Trace Miss Analysis

In the simulation model, the trace miss analysis is performed to estimate the vehicle performance over an aggressive drive cycle such as US06 cycle. In this study, the trace miss is set to be less than 2 mph. As shown in Figure 4-7, once the values of

torque, speed, and power of a motor are calculated based on a given vehicle speed and acceleration from a drive cycle, then they should be compared to the maximum values from given motor specifications. If they are less than maximum values, then the efficiency of motor is calculated by the procedure mentioned in section 4.4. If they exceed the maximum values, it means that the vehicle cannot generate enough power at a given vehicle speed to meet the acceleration required by the drive cycle speed trace.

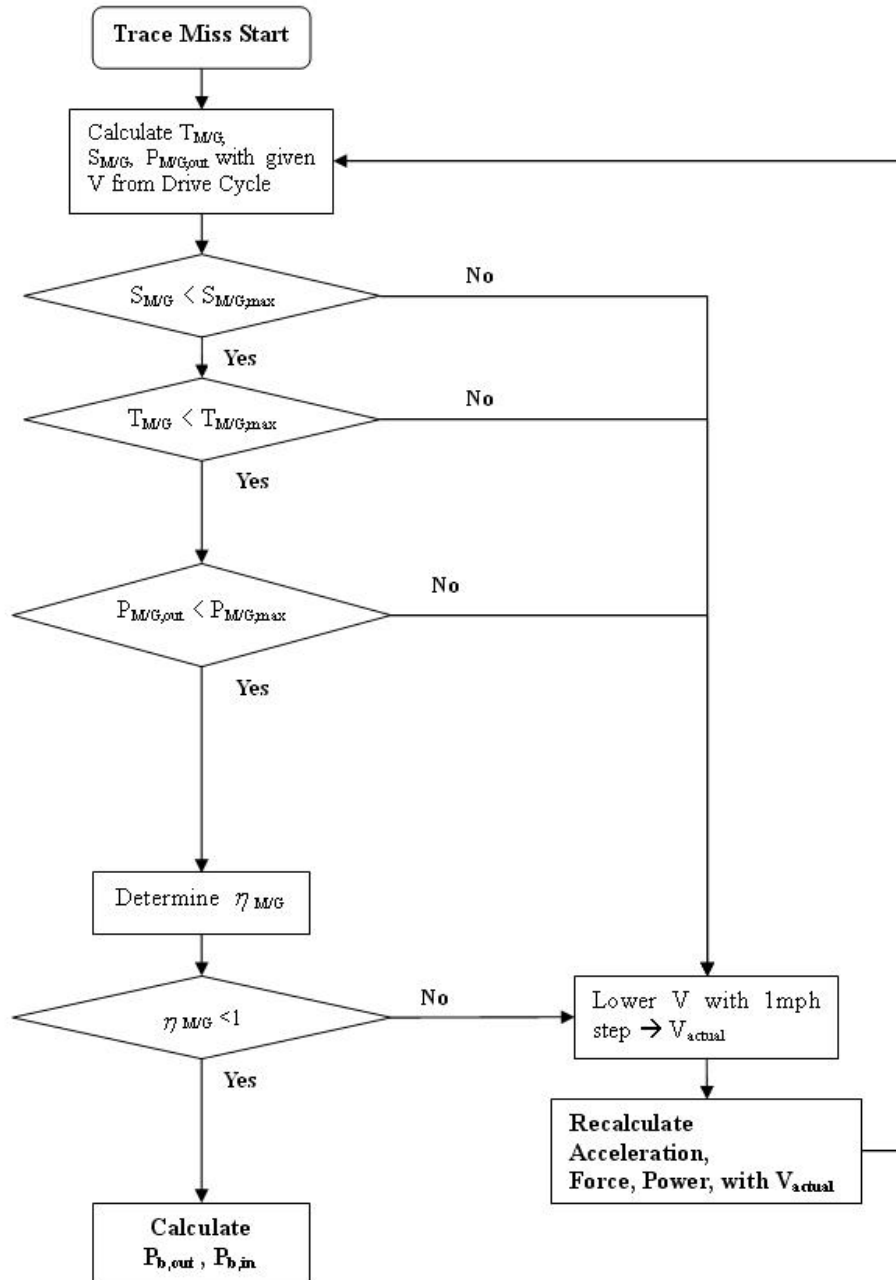


Figure 4-7. Trace miss flowchart

Thus, in this case, the vehicle speed is lowered to an actual vehicle speed, V_{actual} , with 1 mph step. Then, the same procedure is repeated until the values of torque, speed, and power of the motor are less than the maximum values. If the calculated efficiency of the motor is greater than 100 %, then the vehicle speed should be lowered again and the same procedure should be repeated. Finally, the efficiency is determined, then the input and output powers for propulsion and regenerative braking can be calculated. In this process, the difference between the given vehicle speed and the updated actual vehicle speed becomes the trace miss.

4.7 Specifications of Vehicle

A mid-size sport utility vehicle (SUV) is used in this analysis and the specifications are tabulated briefly in Table 4-2. As mentioned in Chapter 3, the manufacture specified value is used for the moment of inertia of the driveline and M/G. Table 4-3 shows motor performance parameters used in the simulation. The acceleration performance result with this particular motor is presented in Table 4-1.

Table 4-2. Mid-size SUV specifications

Vehicle Test Mass, m_v (kg)	1818	Drag Coefficient, C_D	0.417
Frontal Area, A (m ²)	2.686	Rolling Resistance Coefficient, C_{rr}	0.01
Rolling Radius, r_r (m)	0.355	Transmission Gear Ratio, N_t	3.265
Wheel Mass, m_w (kg)	10	Final Drive Gear Ratio, N_f	3.265
Wheel Radius, r_w (m)	0.18	Transmission Efficiency, η_t	0.95
Tire Mass, m_t (kg)	10	Final Drive Gear Efficiency, η_f	0.95
Tire Radius, r_t (m)	0.30	Fraction of Front Braking, f_{fb}	0.6
Moment of Inertia of a wheel/tire, $I_{w/t}$ (kg-m ²)	1.224	Regenerative Brake Fraction, k	0.5
Moment of Inertia of M/G and Driveline, $I_{M/G}N_t^2N_f^2$ (kg-m ²)	5.34		

Table 4-3. Motor performance parameters

Max Torque, T_{max} (N-m)	290.0
Base Motor Speed, S_{base} (rpm)	3000
Max Motor Speed, S_{max} (rpm)	13500
Max Speed Ratio, R	4.50
Power at Base Motor Speed, P_{base} (kW)	91.1

Chapter 5

Results of Power and Energy over Various Drive Cycles

In this analysis, five different drive cycles are used (without grade and towing forces) with vehicle properties described in Tables 4-2 and 4-3. Using vehicle property data, the effective mass of the vehicle is 1.0447 and 1.034 times the test vehicle mass for the on-road and dynamometer tests respectively. The M/G efficiency (including inverter) is based on a map as a function of torque and speed with a peak overall efficiency of 95 % and efficiency at rated power of 85 % (see Table A-1 in Appendix A).

The figures in Chapter 5 are plotted based on Tables A-2 through A-8 in Appendix A. Exact values from simulation results are tabulated in those tables. Note that the rotating inertial energy of the driveline is lumped into that of M/G and the battery losses are not included while the on-road and the single axle dynamometer driving tests are being simulated.

5.1 Propulsion Results over Drive Cycles

In propulsion, AWD, FWD, and RWD vehicles have small differences in powertrain configurations as shown in Figures 4-1, 4-2, and 4-3. The difference among those drive types is that the power from a power source is transmitted to either two axles or one axle. However, if the same efficiencies are assumed for each powertrain, then the overall power transmitted from wheels to ground would be same. Thus, in propulsion case, AWD, FWD and RWD cases have same results with a test vehicle for each test case, such as on-road and dynamometer tests.

5.1.1 On-road Test

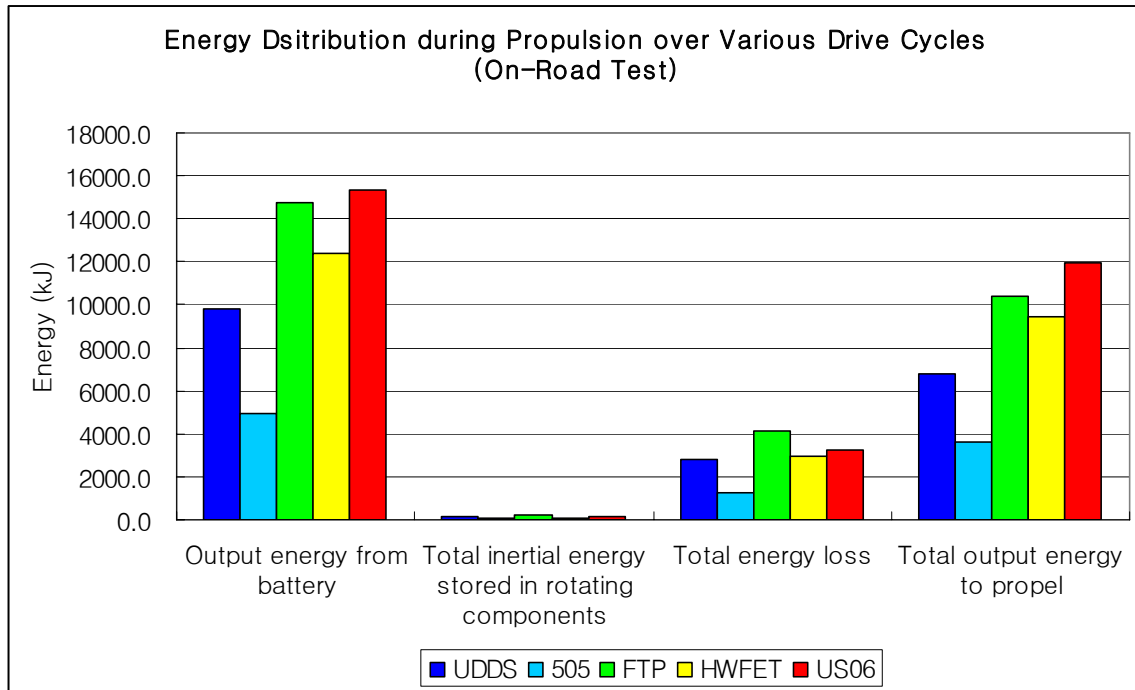


Figure 5-1. Energy distribution during propulsion over various drive cycles (on-road test)

Figure 5-1 shows the energy distribution during propulsion over five different drive cycles for the on-road test case. All output energy from a battery cannot be directly transmitted to wheels. As mentioned previously in Chapter 3, a vehicle has rotating components and they have rotating inertia, so that certain amount of energy is stored in those components during acceleration for propulsion. In Figure 5-1, the amount of that energy is very small, approximately 0.4 – 1.7% of the output energy from a battery, depending on the drive cycle. Also, there is 20 – 28% of energy loss during propulsion. Thus, the rest of energy, which is approximately 70 – 78% of the output energy from a battery, is used to propel the vehicle over drive cycles.

The US06 is the most aggressive drive cycle, so it has the highest peak acceleration and average velocity during propulsion as described in Table 5-1. Hence, in Figure 5-1, the US06 cycle shows largest values of output energy from a battery and total output energy to propel the vehicle even it has a relatively short length of drive cycle.

Table 5-1. Properties of drive cycles used in the analysis

Drive Cycle	Length of drive cycle (sec)	Total Distance of drive cycle (mile)	Peak acceleration (m/s ²)	Average velocity for whole drive cycle (mph)	Average velocity during propulsion (mph)	Propulsion time (sec)	Idle time (sec)
UDDS	1372	7.45	1.48	19.5	26.1	782	261
505	505	3.59	1.48	25.6	34.7	295	99
FTP	2477	11.04	1.48	21.2	28.5	1077	360
HWFET	765	10.25	1.43	48.3	49.8	690	5
US06	596	8.00	3.75	48.4	56.8	429	40

In the FTP and HWFET cycles, they also have large output energy from a battery and total output energy due to a long length of drive cycle, and high average velocity during propulsion respectively.

The energy stored in rotating components during propulsion for the on-road test is shown in Figure 5-2. 52.2% of the rotating inertial energy is stored in the M/G and 47.8% is stored in the wheel/tire assemblies. Note that there is no rotating inertial energy stored in the driveline in Figure 5-2, since the rotating inertia of the driveline is lumped into that of the M/G. The rotating inertial energy storage distribution in each component is same for five different drive cycles with a test vehicle, because it is

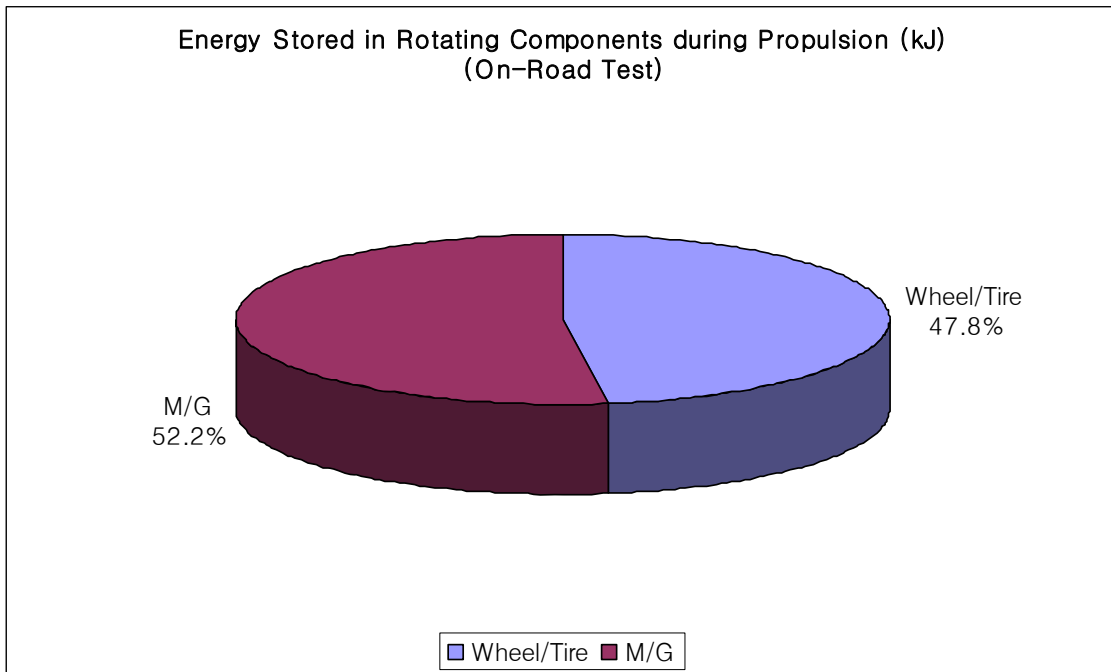


Figure 5-2. Energy stored in rotating components during propulsion over a drive cycle (on-road test)

proportional to rotating inertias of each component and once a vehicle is selected, then the value of rotating inertia is constant.

In Figure 5-1, the total energy loss during propulsion is due to inefficiencies of the final drive gear, the transmission, and the M/G. Table 5-2 below simply shows the fraction of energy loss at each component for five different drive cycles. The driveline losses are 26-40% of total energy loss, and the M/G losses are 60 – 74% of it during propulsion, depending on the drive cycle. In this analysis, it is assumed that the wheel bearing losses are very small, so they are included in driveline losses. The fractions of energy loss at each component are calculated based on Table A-4 in Appendix A.

Table 5-2. Fraction of energy loss at each component during propulsion (on-road test)

Test Case	Type of Drive	Drive Cycle	Energy loss (%)	
			Driveline $E_{\text{driveline,loss}}$	M/G $E_{\text{M/G,loss}}$
On-Road Test	AWD	UDDS	26.4	73.6
		505	30.3	69.7
	FWD	FTP	27.7	72.3
		HWFET	35.0	65.0
	RWD	US06	40.5	59.5

Figure 5-3 shows the energy flow from the battery to the wheel/tire during propulsion over drive cycles for the on-road test case. The output energy comes out from the battery to wheel/tire through the M/G and the driveline. As shown in Figure 5-2, the energy flow becomes lower because a certain amount of energy is stored in rotating components plus losses due to inefficiencies of the M/G and the driveline.

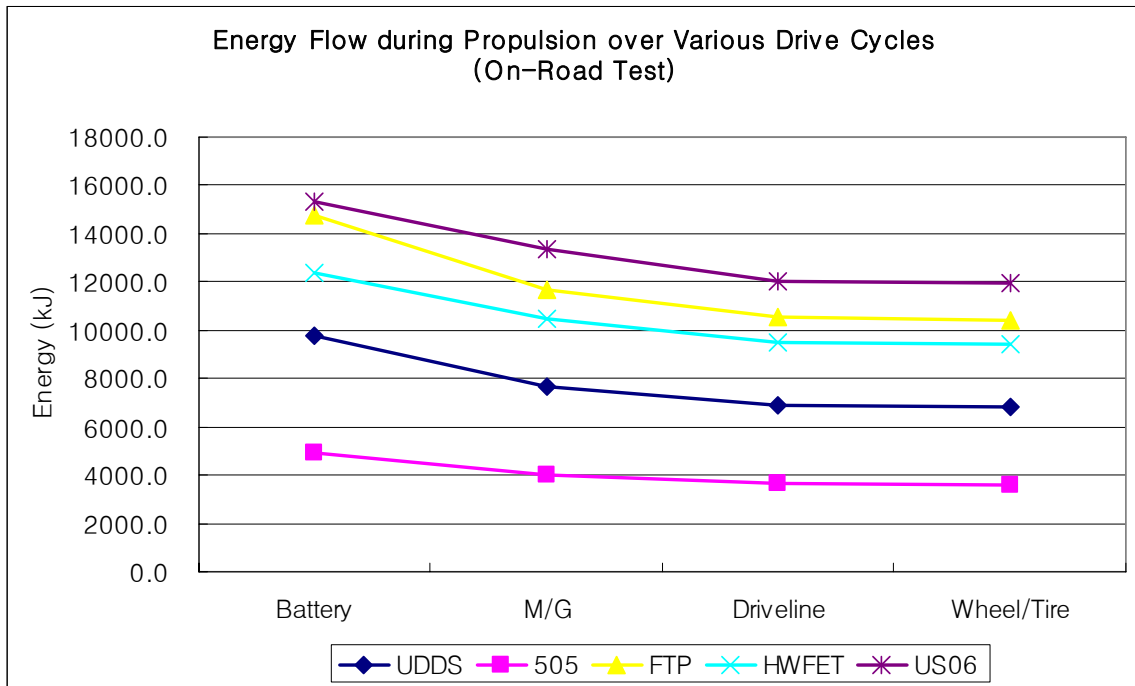


Figure 5-3. Energy flow during propulsion over drive cycles (on-road test)

5.1.2 Dynamometer Test (Single Axle)

In a single axle dynamometer test, Figure 5-4 shows almost the same energy distribution during propulsion over various drive cycles as shown in Figure 5-1. The total output energy to propel for both cases are same, since it represents how much energy a vehicle needs for a drive cycle. However, the other energy values in Figure 5-4 are slightly smaller than that of the on-road test case (see Table A-2 in Appendix A). On a single axle dynamometer, only one axle is rotating and it makes the rotating inertia of wheel/tire assemblies half of that in the on-road test. The difference of total energy required between the two tests in propulsion is approximately 0.5%. Even if the difference is negligibly small in the whole point of view, but it becomes more dominant in terms of rotating inertia.

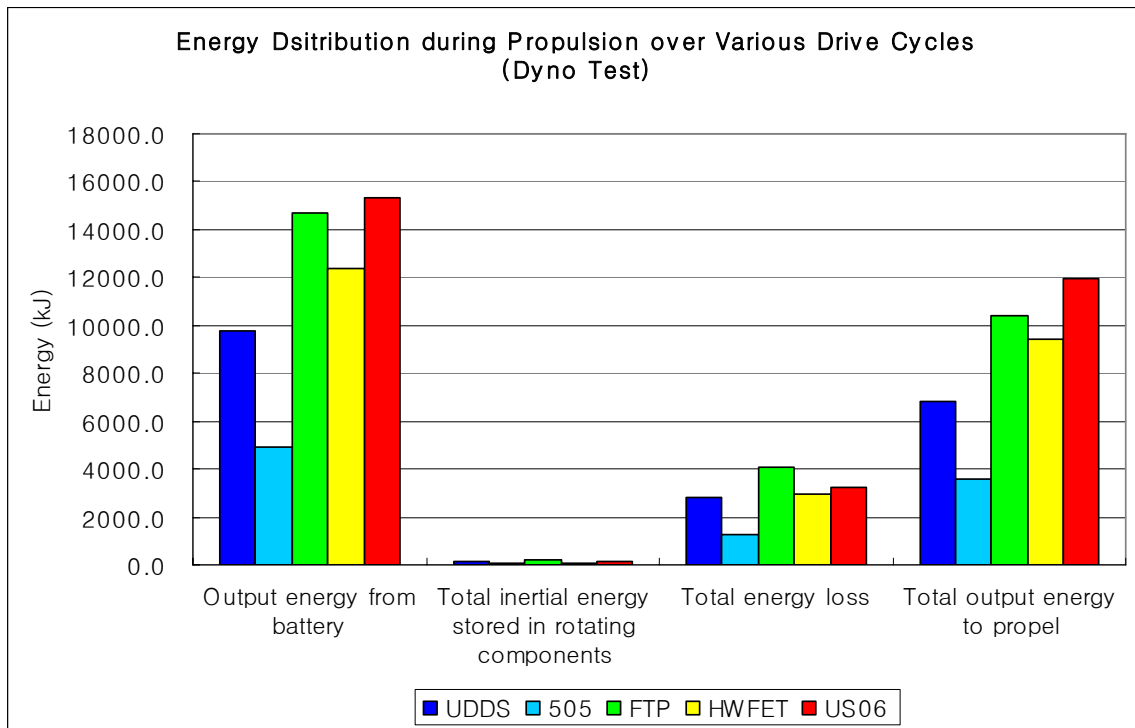


Figure 5-4. Energy distribution during propulsion over various drive cycles (dynamometer test)

The energy stored in rotating components during propulsion for the dynamometer test is shown in Figure 5-5. The value of energy stored in the M/G during propulsion is same, but the value of energy stored in the wheel/tire assemblies reduced to half. Hence,

Figure 5-5 shows that the fraction of it is reduced compared to the on-road test in Figure 5-2.

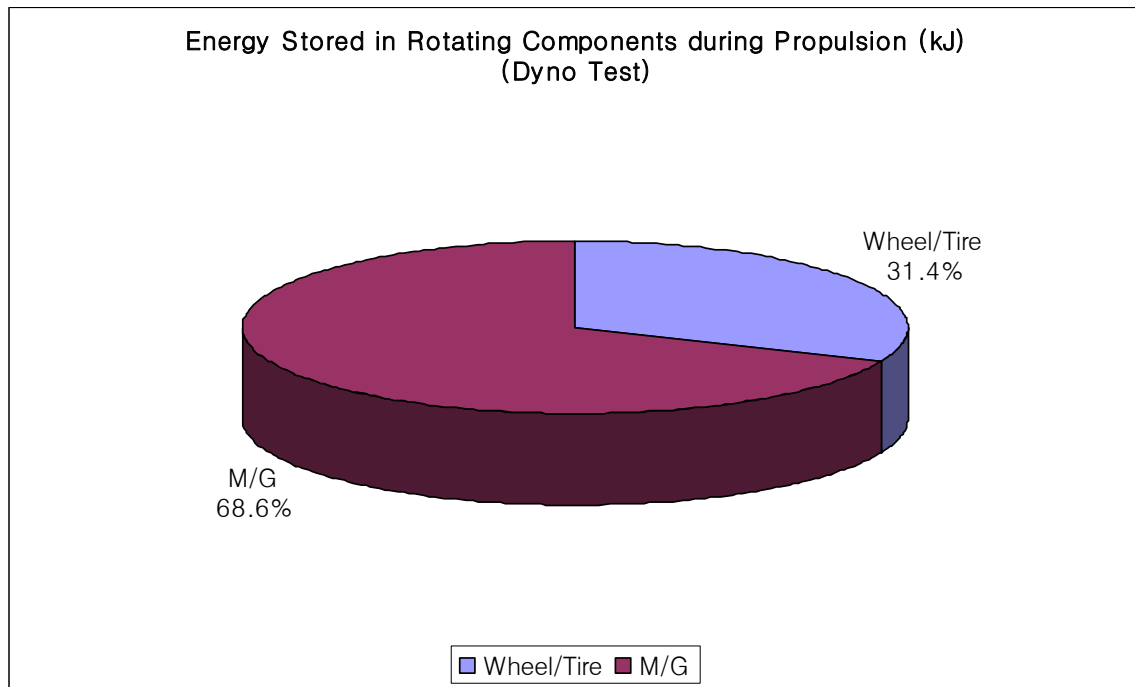


Figure 5-5. Energy stored in rotating components during propulsion over a drive cycle (dynamometer test)

In the dynamometer test, the fractions of energy loss during propulsion at the M/G and the driveline are same as the on-road case as tabulated in Table 5-2. Also, the energy flow from the battery to the wheel/tire during propulsion over drive cycles for the dynamometer test has very similar trends as shown in Figure 5-3 with slightly different values of energy.

5.2 Braking (Regenerative Braking) Results over Drive Cycles

This section presents results of braking case for both the on-road and the single axle dynamometer tests. As described early in Chapter 4, regenerative brake systems usually cannot capture all available energy at wheel/tire assemblies since it has regenerative brake fraction and fractions of front and rear braking. Thus, the AWD, FWD, and RWD vehicles have different results, especially in the on-road test.

5.2.1 On-road Test

Figures 5-6, 5-7, and 5-8 show the energy distribution during braking over various drive cycles for the on-road test with AWD, FWD, and RWD respectively. As shown in Figure 5-6, the AWD case has large amount of energy loss which is approximately 60 – 65% of available energy to be captured at wheel/tire assemblies due to inefficiencies of the M/G and the driveline, and the frictional brake loss.

In Figures 5-7 and 5-8, the available energy to be captured at wheel/tire assemblies is the same as in Figure 5-6. However, in case of FWD and RWD systems, only one axle is directly connected to powertrain and the other axle is not driven. Thus, those two drive systems always have un-driven axle energy loss, so the energy loss of the FWD and the RWD cases is larger than the AWD case. In other words, it means that they can capture less regenerative brake energy than the AWD system. In this analysis, the FWD vehicle captures about 45% less regenerative brake energy and the RWD vehicle captures about 65% less regenerative brake energy than the AWD case in the on-road test. In this comparison, the RWD case has more energy loss than the FWD case because the fraction of rear braking is set up with a smaller value, 0.4, than that of front braking, 0.6, and it increases the un-driven axle energy loss.

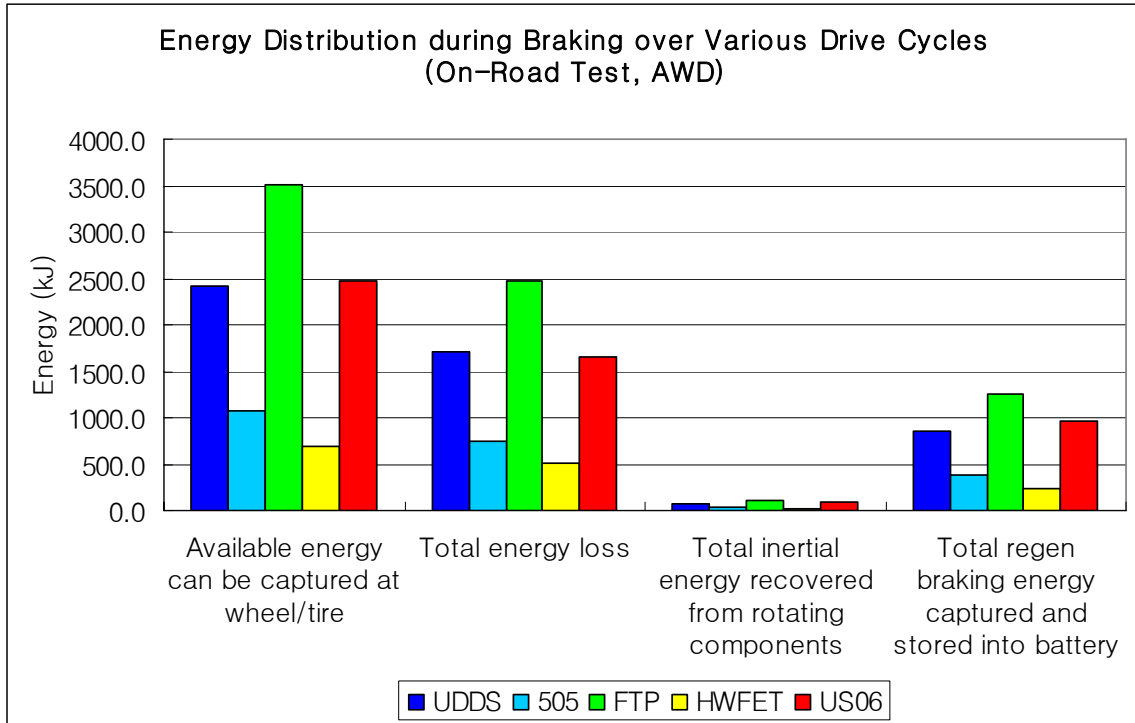


Figure 5-6. Energy distribution during braking over various drive cycles (on-road test, AWD)

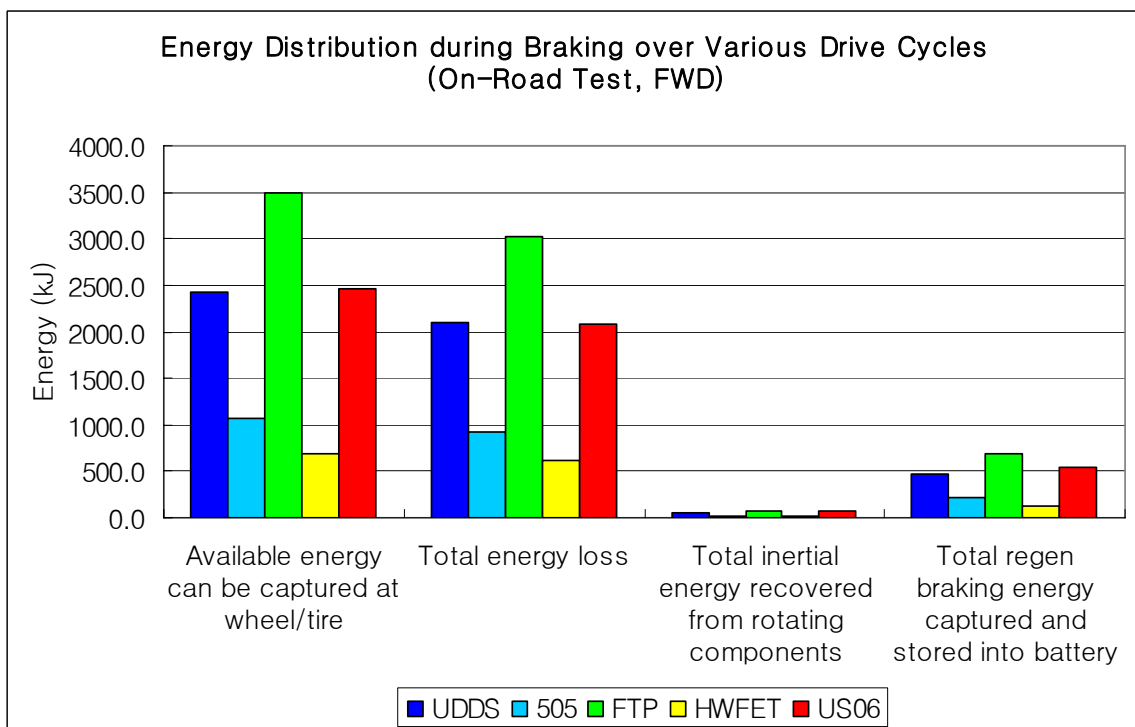


Figure 5-7. Energy distribution during braking over various drive cycles (on-road test, FWD)

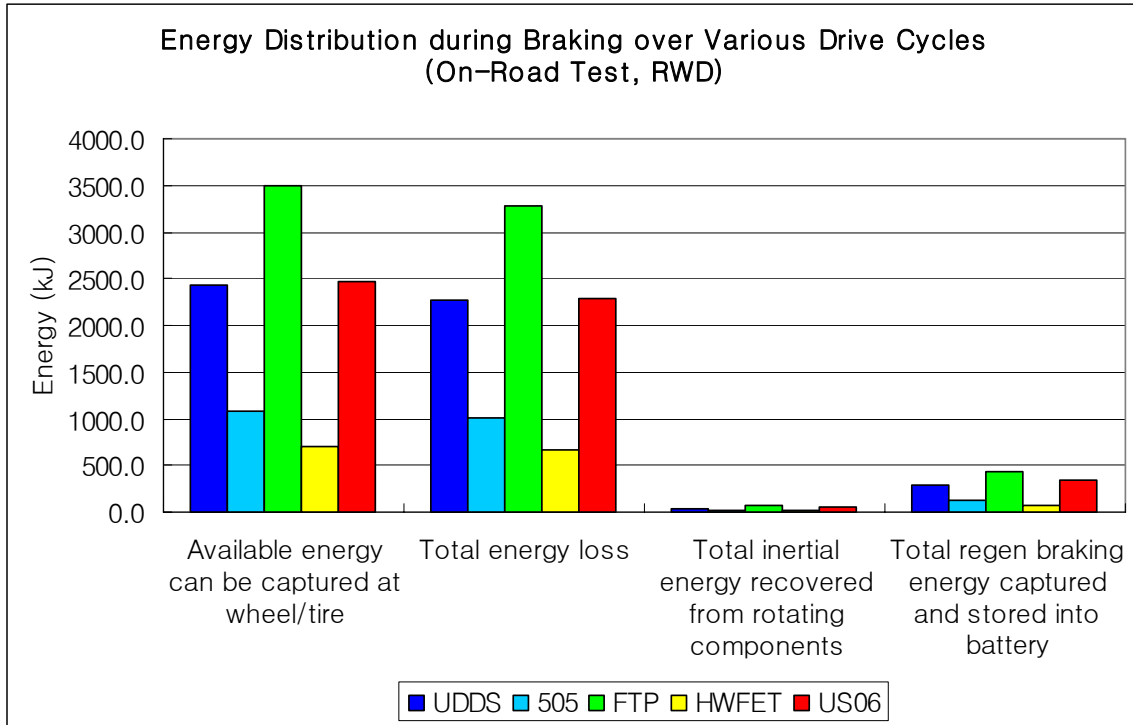


Figure 5-8. Energy distribution during braking over various drive cycles (on-road test, RWD)

Figures 5-9, 5-10, and 5-11 show the regenerative brake energy distribution during braking for the on-road test. The figures are plotted based on Tables A-5 and A-6 in Appendix A. The total regenerative brake energy stored in a battery is mainly captured during braking from two energy sources; translational inertial energy and rotating inertial energy. Most regenerative brake energy is captured from the translational energy. However, in case of the AWD, rotating inertial energy contributes approximately 8 – 9% of total regenerative brake energy, depending on the drive cycle. FWD and RWD vehicles have un-driven axle loss and it reduces the total regenerative brake energy. However, it does not significantly affect the capture of the rotating inertial energy, so the FWD and RWD cases relatively have more contributions such as 11 – 13%, and 14 – 16% of total regenerative brake energy, respectively. Those rotating inertial energy contributions to the total regenerative brake energy are not negligible and should be considered. Note that the FWD and RWD vehicles have only one driven axle, so that the contributions of rotating inertial energy at wheel/tire assemblies is reduced compared to the AWD vehicle case.

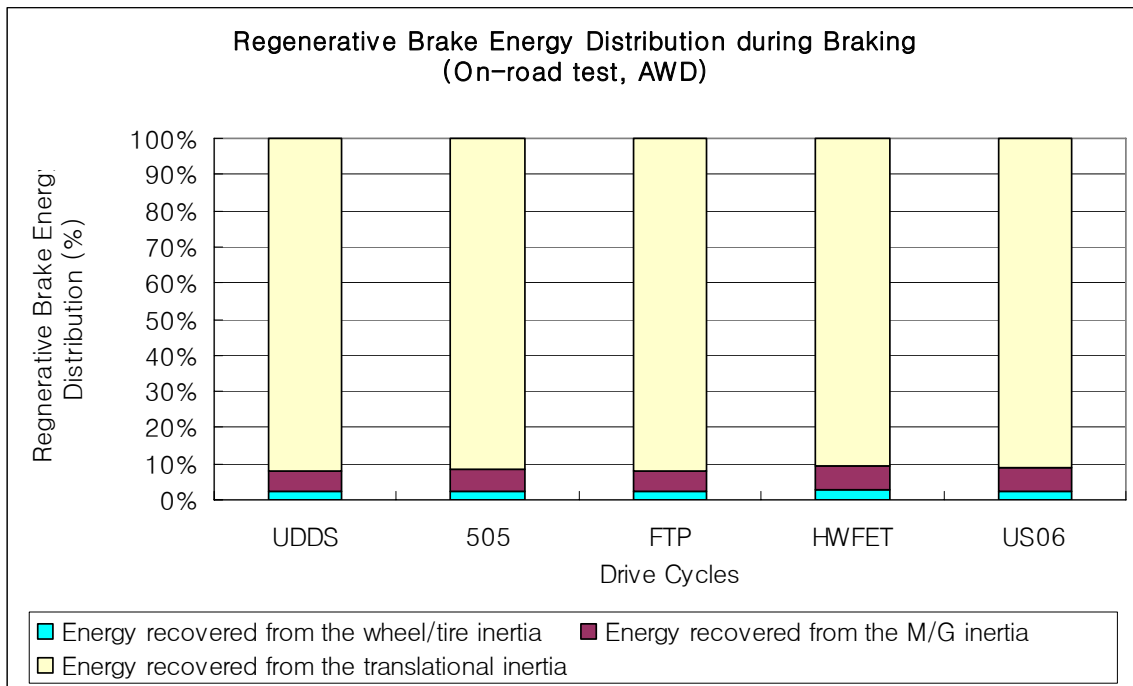


Figure 5-9. Regenerative brake energy distribution during braking (on-road test, AWD)

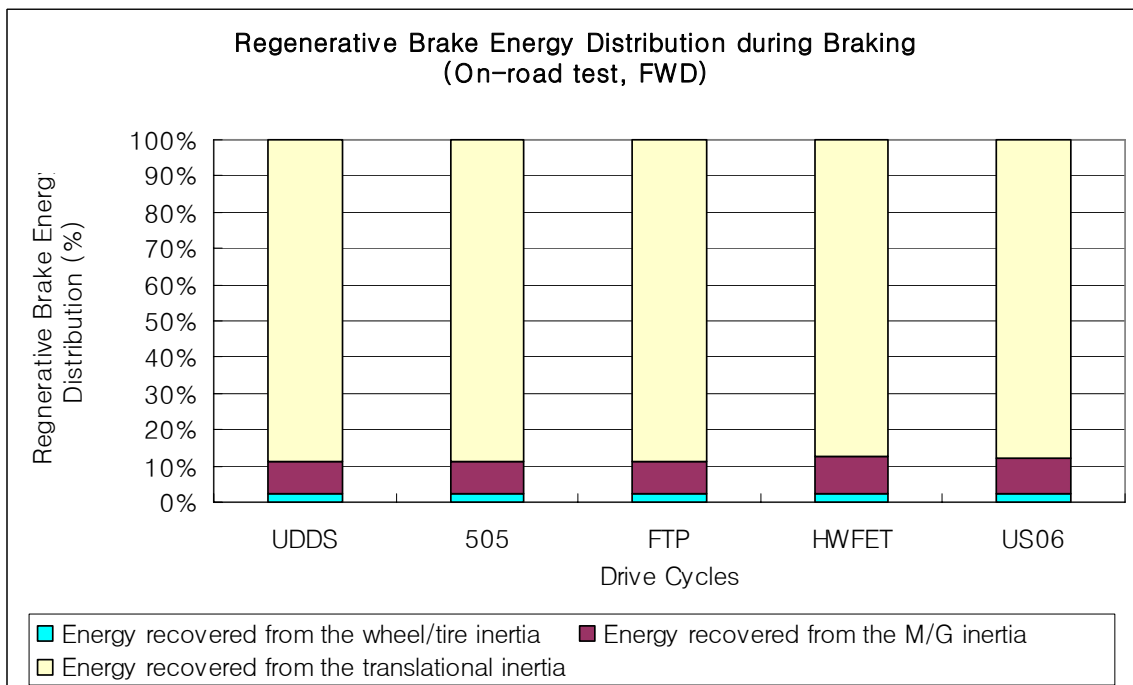


Figure 5-10. Regenerative brake energy distribution during braking (on-road test, FWD)

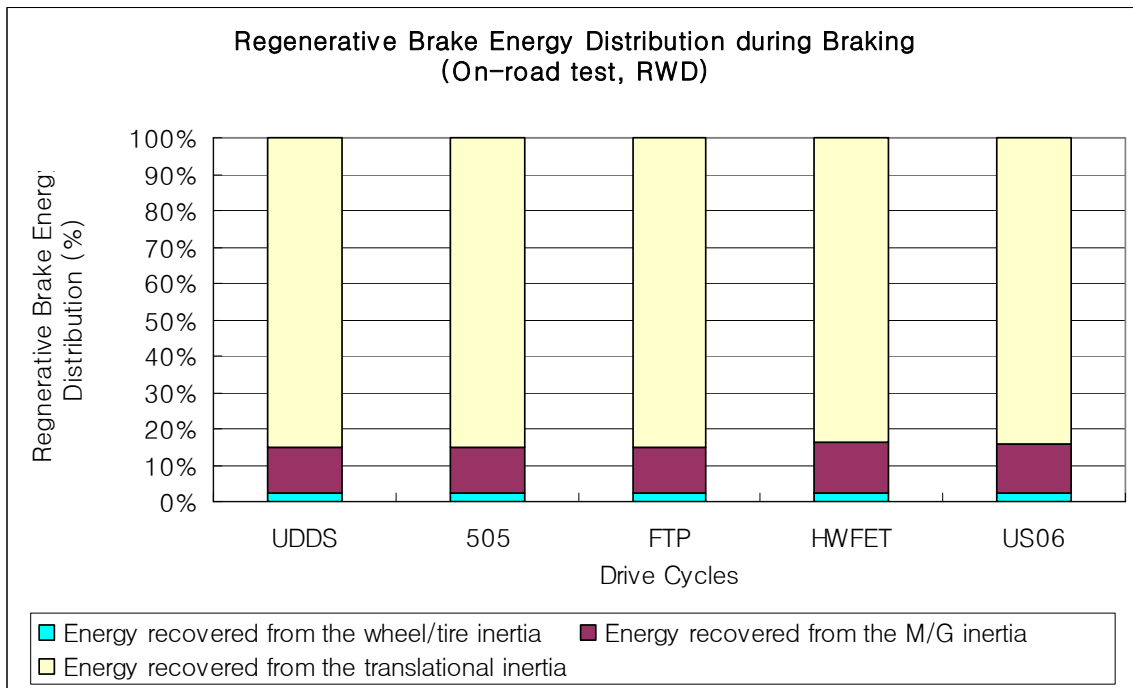


Figure 5-11. Regenerative brake energy distribution during braking (on-road test, RWD)

The energy loss at each component during braking for drive cycles in the on-road test is tabulated in Table A-7 in Appendix A. As shown in the table, the AWD vehicle has less total energy loss than the other two types of vehicle. Based on Table A-7, fractions of energy loss at each component during braking are tabulated in Table 5-3. As discussed previously, the AWD vehicle has no energy loss due to an un-driven axle. Thus, most of energy loss (approximately 72 – 77% and 16 – 22% of total energy loss) comes out from the frictional brakes and the M/G, respectively. However, the FWD and the RWD vehicles have an un-driven axle, so there is un-drive axle energy loss. In Table 5-3, the RWD vehicle has larger fraction of energy loss at the un-driven axle because a front axle is un-driven and the fraction of front brake is usually larger than that of rear one due to safety issues. The fraction of energy loss by the M/G shows some difference depending on the drive cycle, since the M/G efficiency is determined by motor speed and torque as shown in Table A-1 in Appendix A. If the M/G is operating in a relatively high speed and torque region, it has higher efficiency and has less energy loss.

Table 5-3. Fraction of energy loss at each component during braking (on-road test)

Test Case	Type of Drive	Drive Cycle	Energy loss			
			Un-driven Axle $E_{undrivenaxle,loss}$	Friction Brake $E_{brake,loss}$	Driveline $E_{driveline,loss}$	M/G $E_{M/G,loss}$
On-Road Test	AWD	UDDS	0.0%	72.8%	7.1%	20.1%
		505	0.0%	73.6%	7.2%	19.2%
		FTP	0.0%	73.1%	7.1%	19.8%
		HWFET	0.0%	71.5%	7.0%	21.5%
		US06	0.0%	76.8%	7.5%	15.7%
	FWD	UDDS	47.7%	35.8%	3.5%	13.0%
		505	47.9%	35.9%	3.5%	12.7%
		FTP	47.8%	35.8%	3.5%	12.9%
		HWFET	46.8%	35.1%	3.4%	14.8%
		US06	49.0%	36.7%	3.6%	10.7%
	RWD	UDDS	65.7%	21.9%	2.1%	10.3%
		505	65.9%	22.0%	2.1%	10.0%
		FTP	65.8%	21.9%	2.1%	10.2%
		HWFET	64.2%	21.4%	2.1%	12.3%
		US06	66.8%	22.3%	2.2%	8.8%

In Figure 5-12, the energy flow during braking over five different drive cycles are plotted for the on-road test with AWD. All drive cycles show similar trends each other. The first points at wheel/tire represent the available energy to be captured. This energy is increased at brake systems by adding up the rotating inertial energy and it is decreased by friction brake energy loss. In case of FWD and RWD vehicles, additional un-driven axle loss decreases the regenerative brake energy. Then, the energy is again decreased by the driveline and the M/G inefficiencies. Finally, the rest of energy becomes the regenerative brake energy and it is stored in a battery. This trend is similarly observed in FWD and RWD cases.

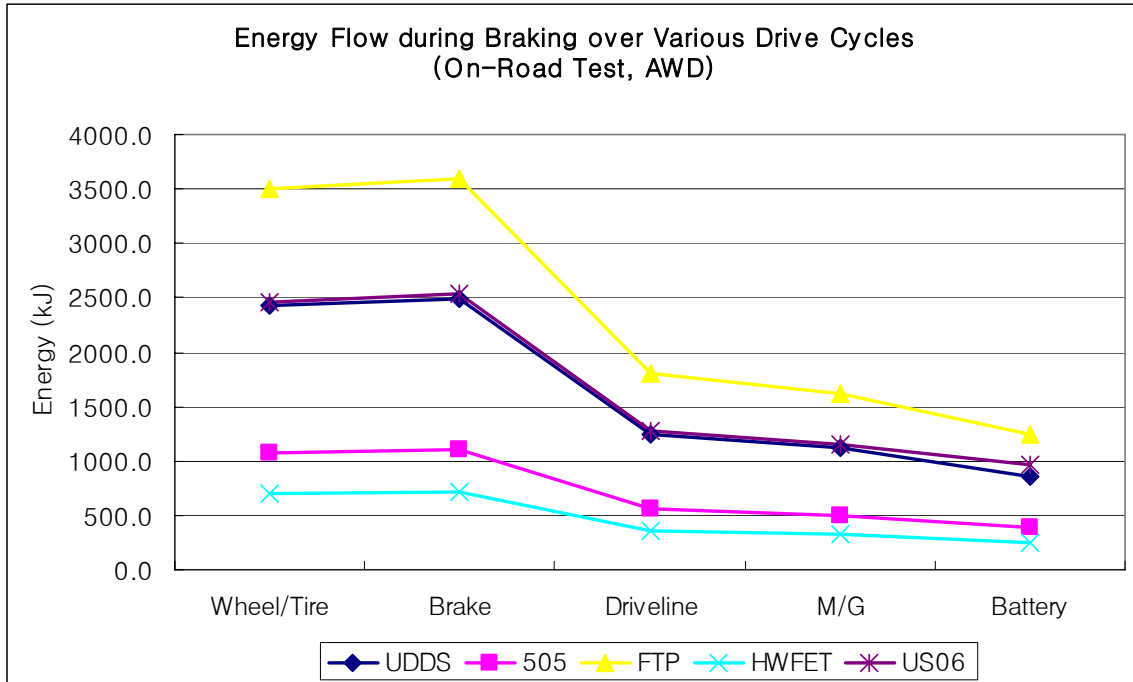


Figure 5-12. Energy flow during braking over drive cycles (on-road test, AWD)

5.2.2 Dynamometer Test (Single Axle)

In the dynamometer test, all drive types of vehicle shows same results during braking over drive cycles, since only one axle is rotating on a single axle dynamometer and all the brake energy should be applied to the driven axle. Figure 5-13 shows the energy distribution during braking over various drive cycles for the dynamometer test. The figure looks almost same as Figure 5-6 for the on-road test with the AWD system. The values of available energy at wheel/tire assemblies for both dynamometer and on-road tests are same, but the other values of dynamometer test are slightly smaller than that of on-road test since only one axle is rotating on a single axle dynamometer and it makes the rotating inertia of wheel/tire assemblies half of that in the on-road test. (see Table A-5 in Appendix A) For example, in the dynamometer test, the values of total regenerative brake energy are approximately 1.5% less than that of the AWD case in the on-road.

In the dynamometer test, the AWD case has almost the same energy distribution as in the on-road test. However, the FWD and RWD have relatively large improvement (~75% for FWD case) in regenerative brake energy capture on a dynamometer compared

to the on-road test results, because all of the braking is now shifted to the driven axle.

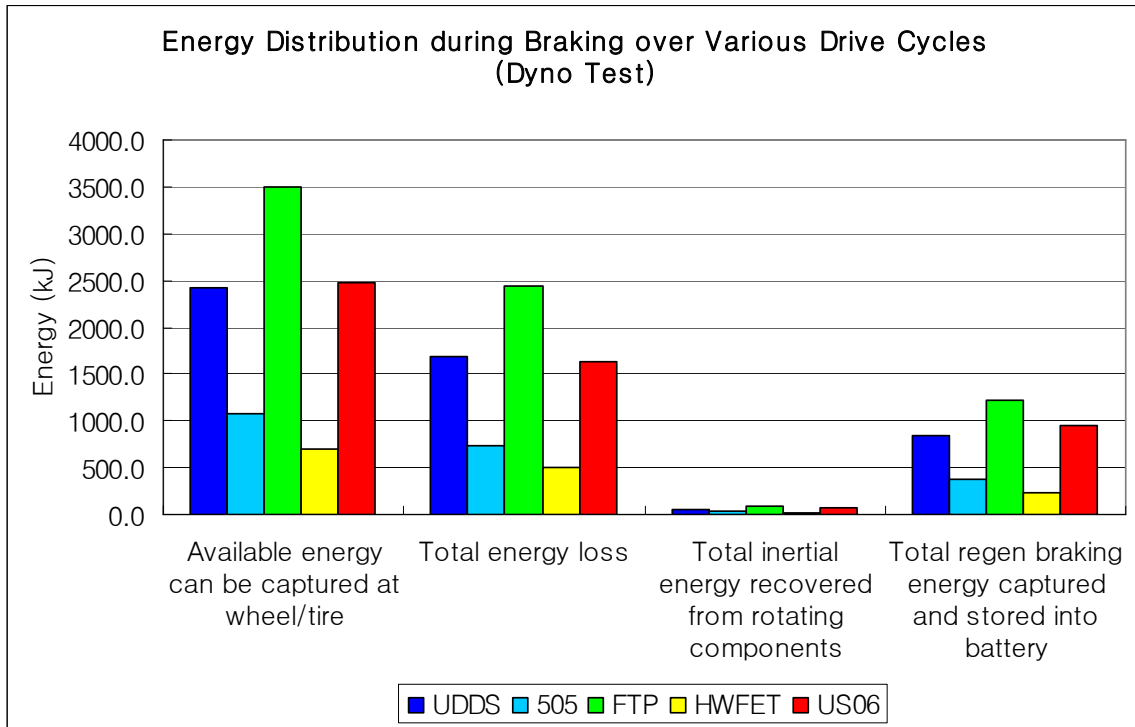


Figure 5-13. Energy distribution during braking over various drive cycles (dynamometer test)

The energy loss at each component during braking and its fraction in the dynamometer test are almost same as the AWD case of on-road test as shown in Tables A-7 and 5-3. However, the FWD and the RWD cases do not have any un-driven axle energy loss in the dynamometer test. Therefore, those two cases have less energy loss than the on-road test cases during braking over drive cycles.

Figure 5-14 shows the regenerative brake energy distribution during braking in the dynamometer test. Again, on a single axle dynamometer, half of rotating inertia of wheel/tire assemblies reduces the portion of regenerative brake energy compared to the AWD case of on-road test. In this analysis, the regenerative brake energy recovered from the wheel/tire assemblies in the dynamometer test is very similar to the values of FWD case in the on-road test. (see Table A-6 in Appendix A)

The energy flow during braking over drive cycles for the dynamometer test has very similar trends as shown in Figure 5-12 with small difference.

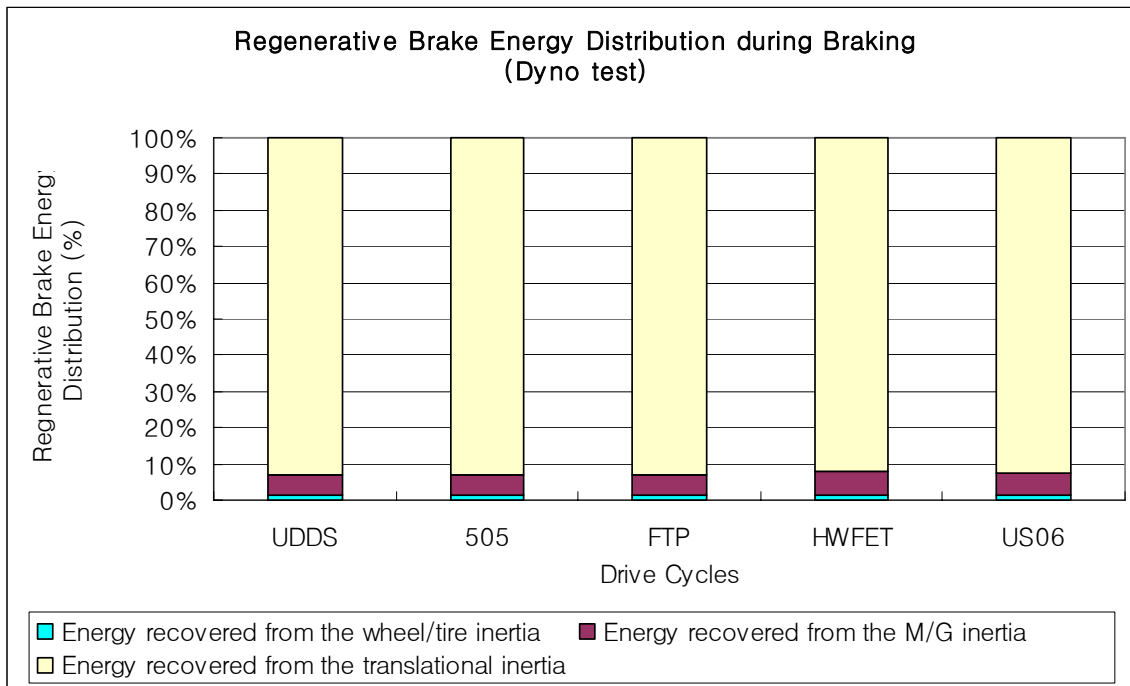


Figure 5-14. Regenerative brake energy distribution during braking (dynamometer test)

5.3 Net Energy Results

The total net energy is obtained by subtracting the regenerative brake energy from the total energy required to propel the vehicle over the drive cycles (see Table A-8 in Appendix A). For example, the AWD vehicle in an on-road test, 9804.1 kJ of energy is required to run the UDDS cycle; but it can capture 857.1 kJ of regenerative brake energy during braking, thus this vehicle needs 8947.0 kJ of net energy to the M/G for the UDDS cycle in an on-road test. Figure 5-15 shows the net energy for on-road and dynamometer tests over various drive cycles based on Table A-8 in Appendix A. In on-road tests, the FWD and the RWD cases need more net energy over drive cycles, because it can capture less regenerative brake energy than the AWD case. In a dynamometer test, the vehicle needs less energy than the AWD vehicle in an on-road test, since it does not have to rotate one axle, but the difference is very small for the AWD vehicles on both tests. Note that the FWD and RWD vehicles in a dynamometer need less net energy compared to the on-road test, since they have not only half rotating inertia, but also have

no un-driven axle loss.

The AWD vehicle uses approximately 2.0 (HWFET) - 8.7 (UDDS) % less net energy and the FWD one approximately 1.0 - 4.9 % less net energy than a vehicle without regenerative braking in an on-road test. In dynamometer tests, all vehicles with regenerative braking use approximately 2.0 - 8.7 % less net energy over the drive cycles.

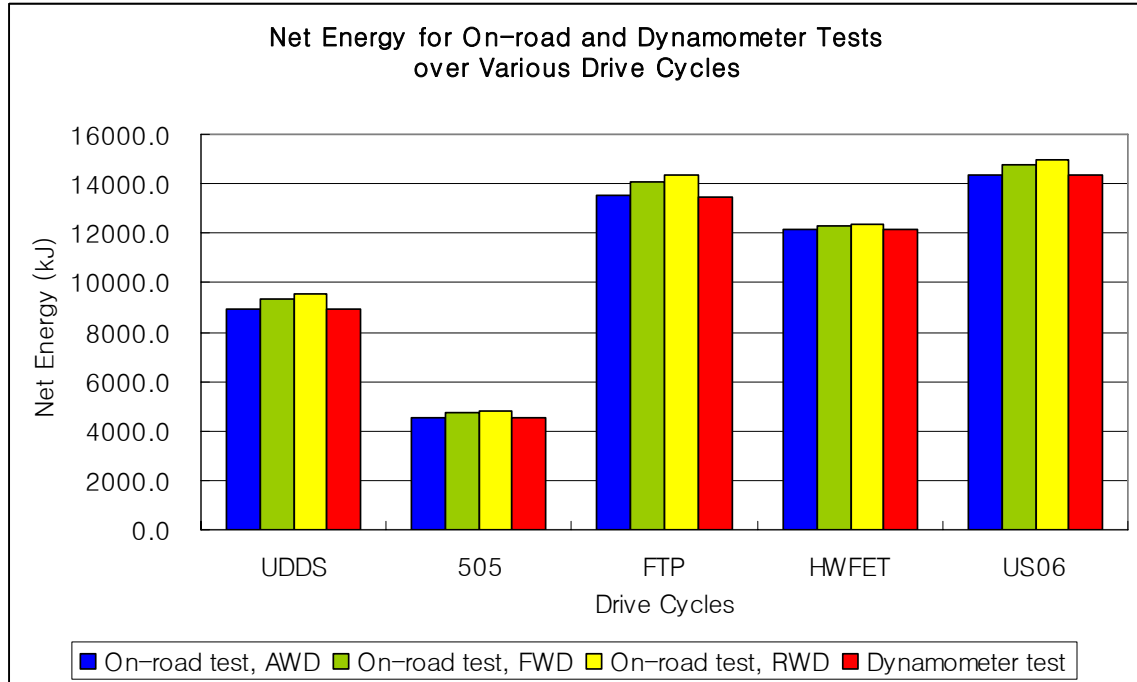


Figure 5-15. Net energy for on-road and dynamometer tests over various drive cycles

Again, as described in Table 5-1, the US06 cycle is more aggressive than the other ones with relatively short length of drive cycle and the highest average velocity during propulsion, so it shows highest net energy required for all tests in Figure 5-15. According to data in Table A-8, the UDDS cycle has highest rate of energy recovery. However, the HWFET cycle shows lowest rate of energy recovery because it is a highway drive cycle, so it has relatively high continuous speed over a drive cycle without much braking.

5.4 Comparison to Results with Two Different Effective Masses

In this analysis, two more cases are simulated with constant mass factors; one is the case with 1.0 of mass factor and the other one is the case with 1.0447 of mass factor for the on-road test. The value of 1.0447 is calculated from the on-road test with given vehicle specifications. The first case represents the test without any inertial mass effect, so that only the test vehicle mass is used over drive cycles. In the second case, 1.0447 of mass factor is directly used as the inertial mass effect instead of using inertial terms separately as shown in Chapter 4. Thus, the inertial term,

$\left(m_v + 4 \frac{I_{w/t}}{r_r^2} + \frac{I_{driveline} N_t^2 N_f^2}{r_r^2} + \frac{I_{M/G} N_t^2 N_f^2}{r_r^2} \right)$, in equation (4-2) is replaced by $1.0447 m_v$.

The detailed results are tabulated in Table A-9 in Appendix A. Table 5-4 shows the comparison of two cases with constant mass factor to the previous case with considering rotating inertia for the on-road test with AWD. The first case shows that the results are smaller than the primary test result because the inertial mass is not considered in this case, so the effective mass is smaller than the other two cases. However, in the second case, the energy required during propulsion is slightly higher and the energy recovered during braking is less than the primary case, which is discussed in this study. It means that there is no significant difference between analyses using an approximated effective mass and using a backward-tracking model developed in this analysis. However, during braking, the energy recovery shows more difference than the required energy during propulsion compared to the case using a backward-tracking model, so it is necessary to account the contribution of rotating inertias in terms of regenerative brake energy.

Table 5-4. Comparison of cases with different constant mass factors to the primary test result (on-road test, AWD) (%)

Test Case	Drive Cycle	Energy Required	Energy Recovered	Net Energy Required
No Rotating Inertia Case with Mass Factor = 1.0	UDDS	98.0%	92.0%	98.5%
	505	98.4%	91.8%	99.0%
	FTP	98.1%	91.9%	98.7%
	HWFET	99.6%	90.6%	99.8%
	US06	98.8%	91.1%	99.3%
No Rotating Inertia with Mass Factor = 1.0447	UDDS	100.6%	97.4%	100.9%
	505	100.5%	97.3%	100.8%
	FTP	100.6%	97.4%	100.8%
	HWFET	100.5%	97.3%	100.5%
	US06	100.4%	97.2%	100.6%

5.5 Additional On-road Test Result for FWD

In this section, an additional on-road test result for FWD is briefly presented using a higher fraction of front braking, 0.8, and a higher regenerative brake fraction, 0.8. Thus, theoretically 64% of brake energy could be captured as stated in the paper by Gao and Ehsani [7]. However, in this test, approximately 46 – 51% of brake energy is captured over various drive cycles due to driveline and motor/generator inefficiencies.

The results of this test for propulsion are the same as that of FWD which is tabulated in Tables A-2 through A-4 in Appendix A. On the other hand, only the results of regenerative braking are changed and the results are tabulated in Tables A-10 through A-13 in Appendix A. Figures 5-16 and 5-17 are plotted based on those tables. Using $f_{fb}=0.8$ and $k=0.8$, the fraction of regenerative brake energy capture during braking is decreased because more translational inertial energy is recovered by higher front brake and regenerative brake fractions as shown in Figure 5-16, but the amount of energy recovered from rotating inertia is increased compared to the previous test result (see Tables A-10 and A-11 in Appendix A). Note that at least 31 kW of peak battery power is required for the US06 cycle to capture this much regenerative brake energy during braking. Also, Figure 5-17 describes that the increase of regenerative brake energy capture using those higher fractions results in the decrease of net energy to propel a vehicle. Thus, it is obvious that the rotating inertia contributes to increase the

regenerative brake energy capture and decrease the net energy over a drive cycle.

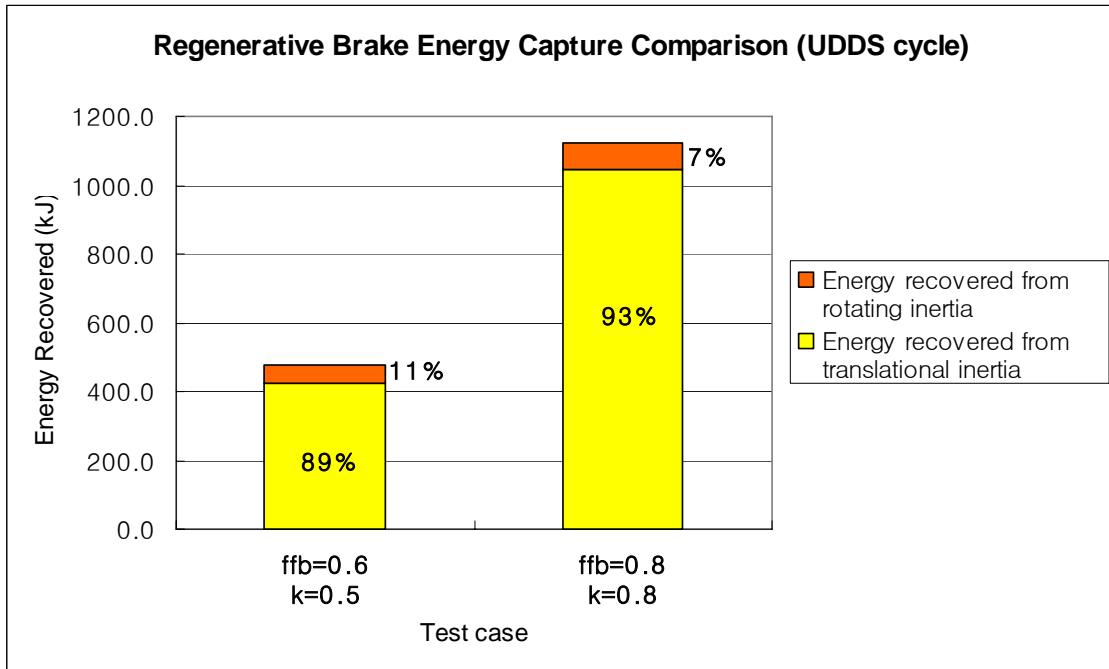


Figure 5-16. Regenerative brake energy capture comparison with the case using $f_{rb}=0.8$ and $k=0.8$ for on-road test with FWD over various drive cycles (UDDS cycle only)

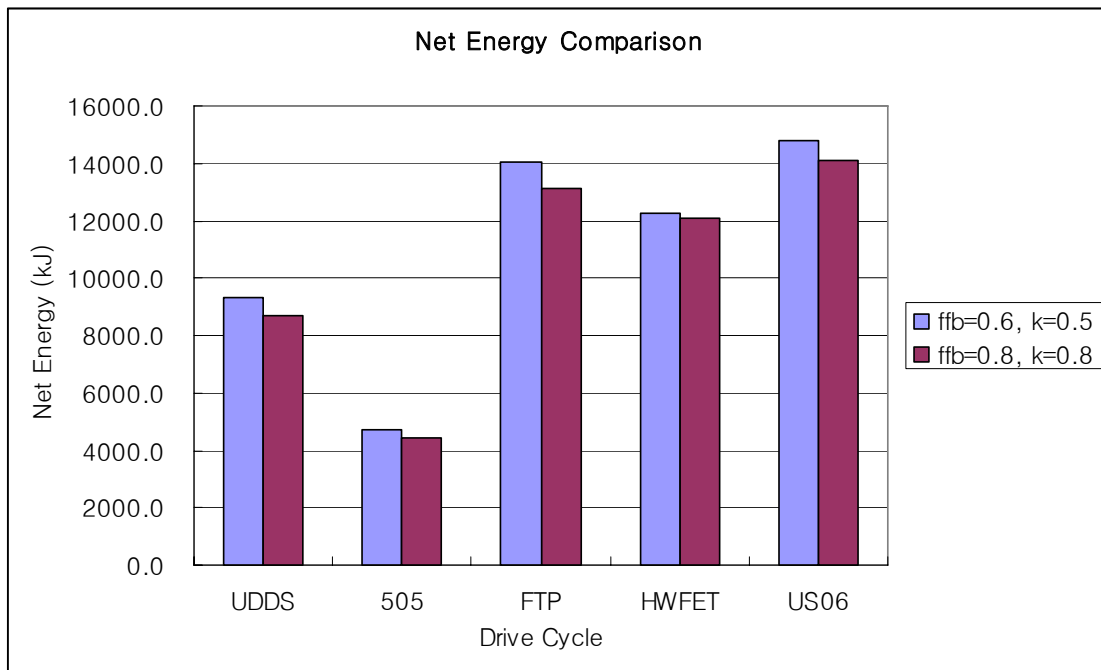


Figure 5-17. Net energy comparison with the case using $f_{rb}=0.8$ and $k=0.8$ for on-road test with FWD over various drive cycles

Chapter 6

Conclusion and Future Work

In this study, a mid-size SUV is simulated to estimate effect of rotating inertias for each component during propulsion and braking over various drive cycles using a backward-tracking simulation model. In propulsion, some amount of energy from the powertrain is stored in rotating components ($\sim 1 - 2$ % of the total propulsion energy) as well as in the inertial mass of the vehicle. In braking, this stored energy discharged by rotating components can be captured by regenerative braking. While the majority of the energy returned from regenerative braking comes from the vehicle inertia, about 8 – 13 % of the total recovered energy is from the rotating components. This contribution from rotating inertias is not negligible, and also is not properly accounted for when a conventional equivalent inertial mass factor is used, even if the difference is very small.

The vehicle inertial energy recovery is limited by a single driven axle (in the case of FWD or RWD) and the regenerative brake fraction, while the rotating inertias are directly coupled to the powertrain. Thus, AWD vehicles have more advantage than FWD and RWD vehicles in terms of regenerative brake energy capture. Also, a higher regenerative brake fraction can reduce the fraction of rotating inertia for total regenerative brake energy capture, but it can increase the total amount of regenerative brake energy capture, because more energy can be captured from translational inertia of a vehicle. However, regenerative braking only cannot be used due to safety issues, so it is necessary to control the blend of regenerative brake and frictional brake systems. In this analysis, a constant regenerative brake fraction which is based on the series regenerative brake strategy is used to simplify the model, but if a more complicated control strategy between frictional braking and regenerative braking is used, then the results could be revised.

For the vehicle and regenerative brake parameters used in this study, going from

an on-road test (two axles) of a FWD vehicle to a single-axle dynamometer test results in over 70 % increase in regenerative brake energy capture due to the concentration of all braking on the driven axle. Also, the energy loss and regenerative brake energy distribution of a FWD and a RWD vehicles show large difference between the on-road and the dynamometer tests. These differences between an on-road and a single axle dynamometer tests for a single axle drive vehicle (FWD or RWD) can be smaller depending on test conditions, but researchers should always notice that there exist such differences due to an un-driven axle on a single axle dynamometer.

As shown in section 5.4, using a proper mass factor gives similar results for energy use, but this study is necessary for estimating the contribution of each rotating inertia. The larger rotating inertias have negative effect in propulsion, since a vehicle consumes more energy to propel, but they also have positive effect in regenerative brake energy capture. Thus, it is important to optimize sizes of rotating components and improve regenerative brake energy capture, so that the vehicle needs less total net energy for fuel economy.

The backward tracking model developed in this study can be used to evaluate the impact of dynamometer testing of vehicles with regenerative braking, and then calibrate an equivalent inertial mass factor. The simulation model in this analysis is based on a pure battery electric powertrain, but is also applicable to hybrid and fuel cell powertrains.

References

- [1] U.S. Environmental Protection Agency (EPA), <http://www.epa.gov>
- [2] Thomas D. Gillespie, *Fundamentals of Vehicle Dynamics*, SAE International, 1992
- [3] John M. Miller, *Propulsion Systems for Hybrid Vehicles*, The Institution of Electrical Engineers, 2004
- [4] Mehrdad Ehsani, Yimin Gao, Sebastien E. Gay, and Ali Emadi, *Modern Electric, Hybrid Electric, and Fuel Cell Vehicles/Fundamentals, Theory, and Design*, CRC Press, 2005
- [5] Gino Sovran, and Dwight Blaser, “A contribution to understanding automotive fuel economy and its limits,” SAE 2003-01-2070
- [6] Yimin Gao, Liping Chen, and Mehrdad Ehsani, “Investigation of the effectiveness of regenerative braking for EV and HEV,” SAE 1999-01-2910
- [7] Yimin Gao, and Mehrdad Ehsani, “Electronic braking system of EV and HEV – integration of regenerative braking, automatic braking force control and ABS,” SAE 2001-01-2478
- [8] Michael Panagiotidis, George Delagrammatikas, and Dennis Assanis, “Development and use of a regenerative braking model for a parallel hybrid electric vehicle,” SAE 2000-01-0995
- [9] Michael Duoba, Theodore Bohn, and Henning Lohse-Busch, “Investigating possible fuel economy bias due to regenerative braking in testing HEVs on 2WD and 4WD chassis dynamometers,” SAE 2005-01-0685
- [10] Stephen W. Moore, Khwaja M. Rahman, and Mehrdad Ehsani, “Effect on vehicle performance of extending the constant power region of electric drive motors,” SAE 1999-01-1152
- [11] A. Rahman, M. Ehsani, and K.L. Butler, “An investigation of electric motor drive characteristics for EV and HEV propulsion system,” SAE 2000-01-3062
- [12] Z. Rahman, K.L. Butler and M. Ehsani, “Effect of extended-speed, constant-power operation of electric drives on the design and performance of EV-HEV propulsion system,” SAE 2000-01-1557
- [13] G.G. Lucas, *Road Vehicle Performance*, Gordon and Breach Science Publishers, 1986

Appendix A: Motor/Controller Efficiency Data and Test Results

Table A-1. Typical motor/controller efficiency data (%)

		Overall Efficiency Map (%)																											
		Motor Speed (RPM)																											
		0	500	1000	1500	2000	2500	3000	3500	4000	4500	5000	5500	6000	6500	7000	7500	8000	8500	9000	9500	10000	10500	11000	11500	12000	12500	13000	13500
Motor Torque (Nm)	0.00	0.0	0.0	0.0	0.0	0.0	0.0	0.0	0.0	0.0	0.0	0.0	0.0	0.0	0.0	0.0	0.0	0.0	0.0	0.0	0.0	0.0	0.0	0.0	0.0	0.0	0.0	0.0	0.0
	12.61	0.0	53.4	67.1	73.4	76.3	79.0	81.0	81.8	82.6	83.4	84.0	85.0	85.5	85.7	86.1	86.5	86.8	87.2	87.7	88.1	88.1	88.4	88.9	89.0	89.2	89.4	89.7	89.9
	25.22	0.0	59.1	71.0	76.1	79.0	80.9	82.2	83.2	84.0	84.7	85.3	85.9	86.4	86.7	87.0	87.2	87.6	87.9	88.3	88.7	89.0	89.7	89.9	90.4	91.0	91.6	91.9	92.4
	37.83	0.0	59.8	73.4	78.5	80.7	82.2	83.3	84.2	85.0	85.6	86.2	86.7	87.3	87.8	88.0	88.2	88.6	88.9	89.3	90.0	90.0	91.2	91.8	92.4	92.7	93.4	93.8	93.9
	50.43	0.0	61.6	74.7	78.9	81.4	83.0	84.2	85.1	85.9	86.5	87.1	87.6	87.9	88.1	88.5	89.0	89.3	90.0	90.5	91.3	91.9	92.5	93.0	93.5	93.9	94.3	94.6	94.7
	63.04	0.0	62.6	74.0	79.4	82.3	83.8	84.7	85.5	86.1	86.7	87.2	87.6	88.2	88.5	88.7	89.1	89.9	90.6	91.6	92.2	92.8	93.4	93.8	94.1	94.3	95.0	95.4	95.7
	75.65	0.0	61.5	75.2	79.4	81.9	83.7	85.0	86.0	86.6	87.1	87.5	87.9	88.4	88.8	89.0	89.4	90.4	91.6	92.4	93.0	93.5	93.8	94.3	94.8				
	88.26	0.0	61.2	74.9	79.5	82.2	84.1	85.5	86.2	86.8	87.4	87.9	88.4	88.9	89.1	89.7	90.3	90.7	92.3	92.8	93.6								
	100.87	0.0	61.1	74.2	79.5	82.2	84.3	85.6	86.3	87.0	87.6	88.2	88.9	89.1	89.5	90.3	90.3	92.0											
	113.48	0.0	61.5	73.6	79.7	82.2	84.3	85.8	86.5	87.2	87.8	88.4	89.1	89.3	89.8	90.6													
	126.09	0.0	59.9	73.3	79.4	82.2	84.1	85.7	86.7	87.3	87.9	88.5	89.2	89.4	90.0														
	138.70	0.0	59.3	73.6	78.8	82.5	84.0	85.5	86.8	87.5	88.0	88.6	89.3																
	151.30	0.0	59.7	72.6	78.7	82.0	84.2	85.4	86.6	87.7	88.2	88.6																	
	163.91	0.0	58.2	72.4	78.9	81.9	84.1	85.7	86.6	87.5	88.4																		
	176.52	0.0	58.3	72.6	78.7	82.0	84.2	85.7	86.8	87.8	88.5																		
	189.13	0.0	57.9	72.3	78.7	81.9	84.4	85.7	86.9	88.0																			
	201.74	0.0	57.6	72.1	78.7	81.9	84.5	85.8	87.0	88.0																			
	214.35	0.0	57.4	71.6	78.4	81.6	84.3	85.6	87.0																				
	226.96	0.0	56.8	71.0	78.0	81.3	84.1	85.4	86.8																				
	239.57	0.0	55.9	70.4	77.5	81.0	83.8	85.2	86.6																				
252.17	0.0	54.9	69.9	76.9	80.6	83.5	85.0																						
264.78	0.0	54.1	69.4	76.4	80.3	83.1	84.8																						
277.39	0.0	53.3	69.1	75.8	80.1	82.7	84.6																						
290.00	0.0	52.6	68.3	75.3	79.9	82.4	84.3																						

Table A-2. Energy required to propel the vehicle at each component over various drive cycles for AWD, FWD, and RWD (kJ)

Test Case	Type of Drive	Drive Cycle	Energy Required to Propel the Vehicle (kJ)			
			Wheel/Tire $E_{w/t,out}$	Driveline $E_{driveline,out}$	M/G $E_{M/G,out}$	Battery $E_{b,out}$
On-Road Test	AWD FWD RWD	UDDS	6818.3	6897.6	7642.7	9804.1
		505	3586.7	3622.2	4013.5	4950.5
		FTP	10405.0	10519.8	11656.3	14754.6
		HWFET	9433.3	9459.8	10481.7	12406.5
		US06	11949.6	12036.6	13336.9	15340.7
Dyno Test	AWD FWD RWD	UDDS	6818.3	6857.9	7598.8	9751.1
		505	3586.7	3604.4	3993.8	4926.4
		FTP	10405.0	10462.4	11592.7	14677.6
		HWFET	9434.0	9447.1	10467.7	12394.1
		US06	11949.6	11993.1	13288.7	15294.1

Table A-3. Energy stored in rotating components due to rotating inertia at each component during propulsion over various drive cycles for AWD, FWD, and RWD (kJ)

Test Case	Type of Drive	Drive Cycle	Energy Stored in Rotating Components due to Rotating Inertia			
			Wheel/Tire $E_{w/t,I}$	Driveline $E_{driveline,I}$	M/G $E_{M/G,I}$	Total $E_{total,I}$
On-Road Test	AWD FWD RWD	UDDS	79.3	0.0	86.5	165.8
		505	35.5	0.0	38.7	74.2
		FTP	114.8	0.0	125.2	240.0
		HWFET	26.5	0.0	28.9	55.4
		US06	87.0	0.0	94.8	181.8
Dyno Test	AWD FWD RWD	UDDS	39.7	0.0	86.5	126.1
		505	17.7	0.0	38.7	56.5
		FTP	57.4	0.0	125.2	182.6
		HWFET	13.0	0.0	28.5	41.5
		US06	43.5	0.0	94.8	138.3

Table A-4. Energy loss at each component during propulsion over various drive cycles for AWD, FWD, and RWD (kJ)

Test Case	Type of Drive	Drive Cycle	Energy Loss		
			Driveline $E_{\text{driveline,loss}}$	M/G $E_{\text{M/G,loss}}$	Total $E_{\text{total,loss}}$
On-Road Test	AWD FWD RWD	UDDS	745.2	2074.8	2820.0
		505	391.3	898.3	1289.6
		FTP	1136.5	2973.1	4109.6
		HWFET	1022.0	1895.8	2917.8
		US06	1300.3	1908.9	3209.3
Dyno Test	AWD FWD RWD	UDDS	740.9	2065.8	2806.7
		505	389.4	893.9	1283.3
		FTP	1130.3	2959.7	4090.0
		HWFET	1020.6	1898.0	2918.6
		US06	1295.7	1910.6	3206.2

Table A-5. Regenerative brake energy at each component during braking over various drive cycles (kJ)

Test Case	Type of Drive	Drive Cycle	Brake Energy	Regenerative Brake Energy			
			Wheel/Tire $E_{\text{w/t,in}}$	Brake $E_{\text{brake,in}}$	Driveline $E_{\text{driveline,in}}$	M/G $E_{\text{M/G,in}}$	Battery $E_{\text{b,in}}$
On-Road Test	AWD	UDDS	2426.3	2495.1	1247.6	1125.9	857.1
		505	1075.4	1106.8	553.4	499.5	389.3
		FTP	3501.7	3602.0	1801.0	1625.4	1246.4
		HWFET	695.2	720.4	360.2	325.1	244.3
		US06	2466.4	2542.2	1271.1	1147.1	970.1
	FWD	UDDS	2426.3	1497.1	748.5	675.6	478.9
		505	1075.4	664.1	332.0	299.7	216.5
		FTP	3501.7	2161.2	1080.6	975.2	695.4
		HWFET	695.2	432.2	216.1	195.1	131.5
		US06	2466.4	1525.3	762.6	688.3	549.3
	RWD	UDDS	2426.3	998.1	499.0	450.4	291.5
		505	1075.4	442.7	221.4	199.8	133.4
		FTP	3501.7	1440.8	720.4	650.2	424.9
		HWFET	695.2	288.2	144.1	130.0	74.6
		US06	2466.4	1016.9	508.4	458.9	341.5
Dyno Test	AWD FWD RWD	UDDS	2426.3	2460.7	1230.4	1110.4	844.6
		505	1075.4	1091.1	545.6	492.4	383.5
		FTP	3501.7	3551.8	1775.9	1602.8	1228.1
		HWFET	696.0	708.4	354.2	319.7	240.0
		US06	2466.4	2504.3	1252.1	1130.1	954.8

Table A-6. Energy recovered from rotating inertia at each component during braking over various drive cycles (kJ)

Test Case	Type of Drive	Drive Cycle	Energy Recovered in Rotating Components due to Rotating Inertia			
			Wheel/Tire $E_{w/t,I}$	Driveline $E_{driveline,I}$	M/G $E_{M/G,I}$	Total $E_{total,I}$
On-Road Test	AWD	UDDS	20.2	0.0	48.9	69.1
		505	9.4	0.0	22.7	32.0
		FTP	29.6	0.0	71.5	101.1
		HWFET	6.6	0.0	16.0	22.6
		US06	24.9	0.0	60.3	85.2
	FWD	UDDS	10.7	0.0	43.0	53.6
		505	4.9	0.0	19.7	24.6
		FTP	15.6	0.0	62.7	78.2
		HWFET	3.3	0.0	13.3	16.6
		US06	13.1	0.0	52.6	65.7
	RWD	UDDS	6.1	0.0	37.0	43.2
		505	2.8	0.0	17.2	20.0
		FTP	9.0	0.0	54.2	63.2
		HWFET	1.7	0.0	10.5	12.3
		US06	7.6	0.0	45.7	53.2
Dyno Test	AWD FWD RWD	UDDS	10.1	0.0	48.7	58.7
		505	4.7	0.0	22.6	27.2
		FTP	14.7	0.0	71.2	86.0
		HWFET	3.3	0.0	15.9	19.2
		US06	12.4	0.0	60.0	72.4

Table A-7. Energy loss at each component during braking over various drive cycles (kJ)

Test Case	Type of Drive	Drive Cycle	Energy loss				
			Undriven Axle $E_{undrivenaxle,loss}$	Friction Brake $E_{brake,loss}$	Driveline $E_{driveline,loss}$	M/G $E_{M/G,loss}$	Total $E_{total,loss}$
On-Road Test	AWD	UDDS	0.0	1247.6	121.6	344.0	1713.2
		505	0.0	553.4	54.0	144.4	751.8
		FTP	0.0	1801.0	175.6	488.3	2464.9
		HWFET	0.0	360.2	35.1	108.2	503.5
		US06	0.0	1271.1	123.9	259.6	1654.6
	FWD	UDDS	998.1	748.5	73.0	271.7	2091.3
		505	442.7	332.0	32.4	117.4	924.6
		FTP	1440.8	1080.6	105.4	389.1	3015.9
		HWFET	288.2	216.1	21.1	91.0	616.4
		US06	1016.9	762.6	74.4	221.6	2075.5
	RWD	UDDS	1497.1	499.0	48.7	234.0	2278.7
		505	664.1	221.4	21.6	100.6	1007.6
		FTP	2161.2	720.4	70.2	334.6	3286.4
		HWFET	432.2	144.1	14.0	82.9	673.2
		US06	1525.3	508.4	49.6	199.9	2283.2
Dyno Test	AWD	UDDS	0.0	1230.4	120.0	340.9	1691.2
		505	0.0	545.6	53.2	143.1	741.9
	RWD	FTP	0.0	1775.9	173.2	484.0	2433.1
		HWFET	0.0	354.2	34.5	106.6	495.4
		US06	0.0	1252.1	122.1	257.8	1632.0

Table A-8. Net energy over drive cycles (kJ)

Test Case	Type of Drive	Drive Cycle	Energy Required	Energy Recovered	Net Energy Required
On-Road Test	AWD	UDDS	9804.1	857.1	8947.0
		505	4950.5	389.3	4561.2
		FTP	14754.6	1246.4	13508.2
		HWFET	12406.5	244.3	12162.1
		US06	15340.7	970.1	14370.5
	FWD	UDDS	9804.1	478.9	9325.2
		505	4950.5	216.5	4734.0
		FTP	14754.6	695.4	14059.2
		HWFET	12406.5	131.5	12275.0
		US06	15340.7	549.3	14791.4
	RWD	UDDS	9804.1	291.5	9512.6
		505	4950.5	133.4	4817.1
		FTP	14754.6	424.9	14329.7
		HWFET	12406.5	74.6	12331.8
		US06	15340.7	341.5	14999.2
Dyno Test	AWD	UDDS	9751.1	844.6	8906.5
		505	4926.4	383.5	4542.9
		FTP	14677.6	1228.1	13449.5
		HWFET	12394.1	240.0	12154.1
		US06	15294.1	954.8	14339.3

Table A-9. Other cases with different constant mass factors (on-road test, AWD) (kJ)

Test Case	Drive Cycles	Energy Required	Energy Recovered	Net Energy Required
Primary Case (On-road test, AWD)	UDDS	9804	857	8947
	505	4951	389	4561
	FTP	14755	1246	13508
	HWFET	12406	244	12162
	US06	15341	970	14371
No Rotating Inertia Case with Mass Factor = 1.0	UDDS	9605	788	8816
	505	4871	357	4514
	FTP	14476	1146	13331
	HWFET	12356	221	12135
	US06	15157	884	14273
No Rotating Inertia Case with Mass Factor = 1.0447	UDDS	9860	835	9025
	505	4976	379	4597
	FTP	14836	1214	13622
	HWFET	12463	238	12225
	US06	15406	943	14463

Table A-10. Regenerative brake energy at each component during braking over various drive cycles with higher fraction of front braking and regenerative brake fraction ($f_{fb}=0.8$ and $k=0.8$) (kJ)

Test Case	Type of Drive	Drive Cycle	Brake Energy	Regenerative Brake Energy			
			Wheel/Tire $E_{w/t,in}$	Brake $E_{brake,in}$	Driveline $E_{driveline,in}$	M/G $E_{M/G,in}$	Battery $E_{b,in}$
On-road Test	FWD	UDDS	2426.3	1996.1	1596.9	1441.2	1122.8
		505	1075.4	885.5	708.4	639.3	509.6
		FTP	3501.7	2881.6	2305.3	2080.5	1632.4
		HWFET	695.2	576.3	461.1	416.1	324.5
		US06	2466.4	2033.7	1627.0	1468.3	1260.5

Table A-11. Energy recovered from rotating inertia at each component during braking over various drive cycles with higher fraction of front braking and regenerative brake fraction ($f_{fb}=0.8$ and $k=0.8$) (kJ)

Test Case	Type of Drive	Drive Cycle	Energy Recovered in Rotating Components due to Rotating Inertia			
			Wheel/Tire $E_{w/t,I}$	Driveline $E_{driveline,I}$	M/G $E_{M/G,I}$	Total $E_{total,I}$
On-road Test	FWD	UDDS	27.1	0.0	51.2	78.3
		505	12.6	0.0	23.8	36.4
		FTP	39.7	0.0	75.0	114.7
		HWFET	9.1	0.0	17.2	26.3
		US06	33.4	0.0	63.0	96.3

Table A-12. Energy loss at each component during braking over various drive cycles with higher fraction of front braking and regenerative brake fraction ($f_{fb}=0.8$ and $k=0.8$) (kJ)

Test Case	Type of Drive	Drive Cycle	Energy loss				
			Undriven Axle $E_{undrivenaxle,loss}$	Friction Brake $E_{brake,loss}$	Driveline $E_{driveline,loss}$	M/G $E_{M/G,loss}$	Total $E_{total,loss}$
On-road Test	FWD	UDDS	499.0	399.2	155.7	393.5	1447.4
		505	221.4	177.1	69.1	163.9	631.4
		FTP	720.4	576.3	224.8	557.4	2078.9
		HWFET	144.1	115.3	45.0	119.0	423.3
		US06	508.4	406.7	158.6	290.5	1364.3

Table A-13. Net energy over drive cycles with higher fraction of front braking and regenerative brake fraction ($f_{fb}=0.8$ and $k=0.8$) (kJ)

Test Case	Type of Drive	Drive Cycle	Energy Required	Energy Recovered	Net Energy Required
On-road Test	FWD	UDDS	9751.1	844.6	8906.5
		505	4926.4	383.5	4542.9
		FTP	14677.6	1228.1	13449.5
		HWFET	12394.1	240.0	12154.1
		US06	15294.1	954.8	14339.3

Appendix B: Drive Cycles

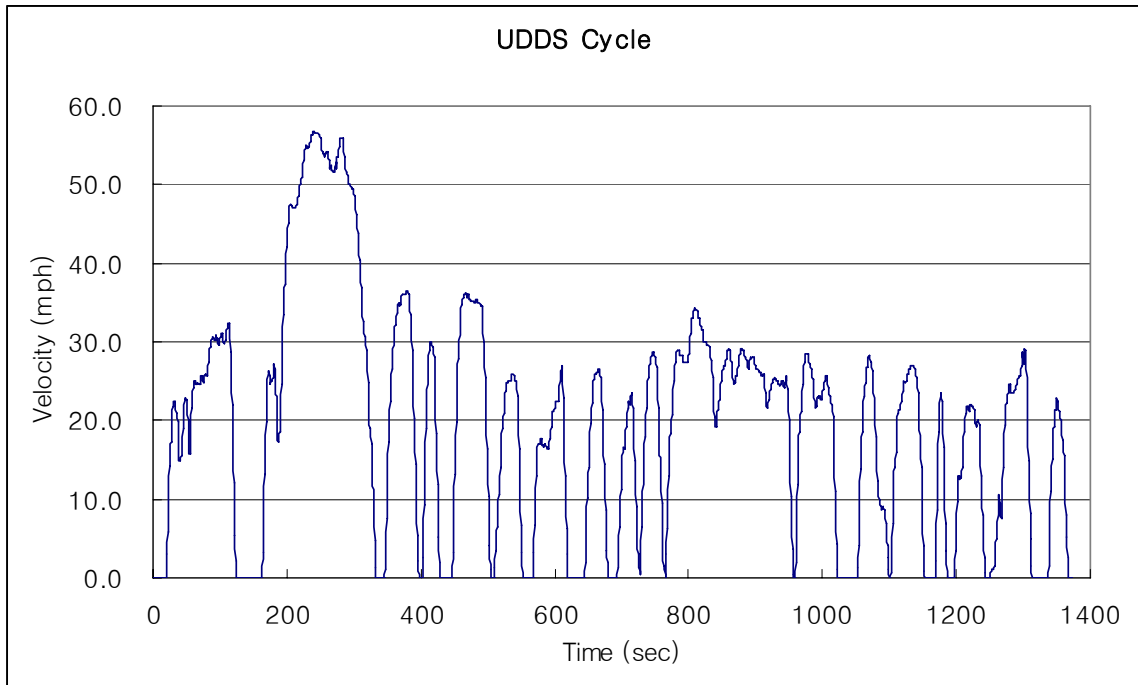


Figure B-1. UDDS cycle

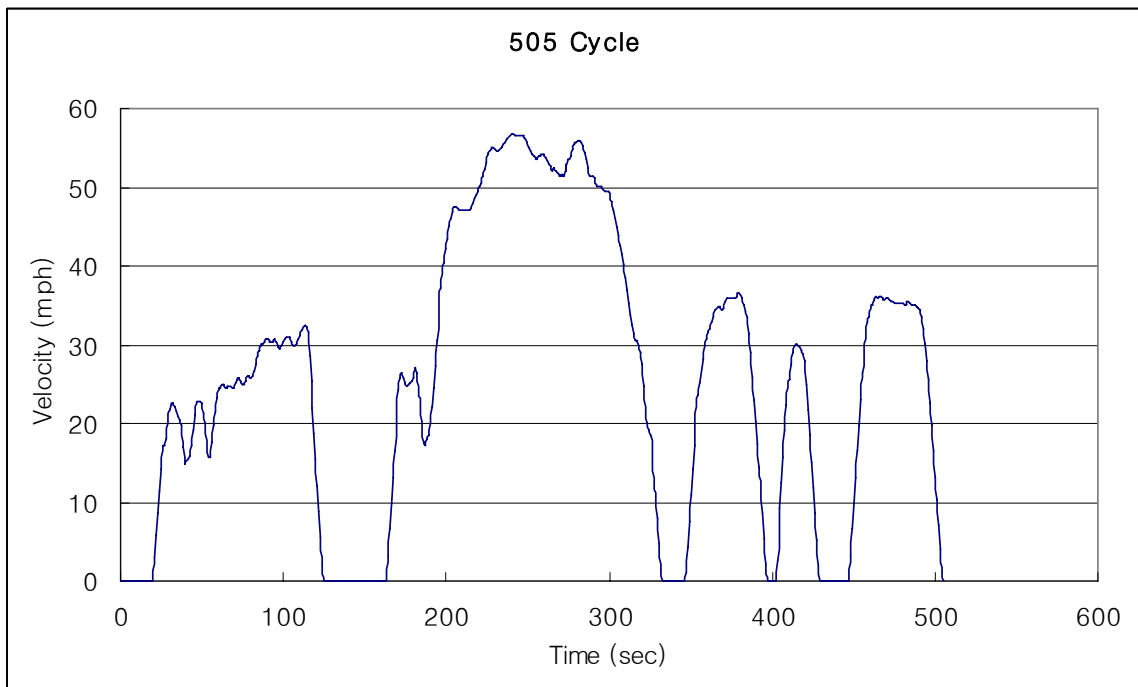


Figure B-2. 505 cycle

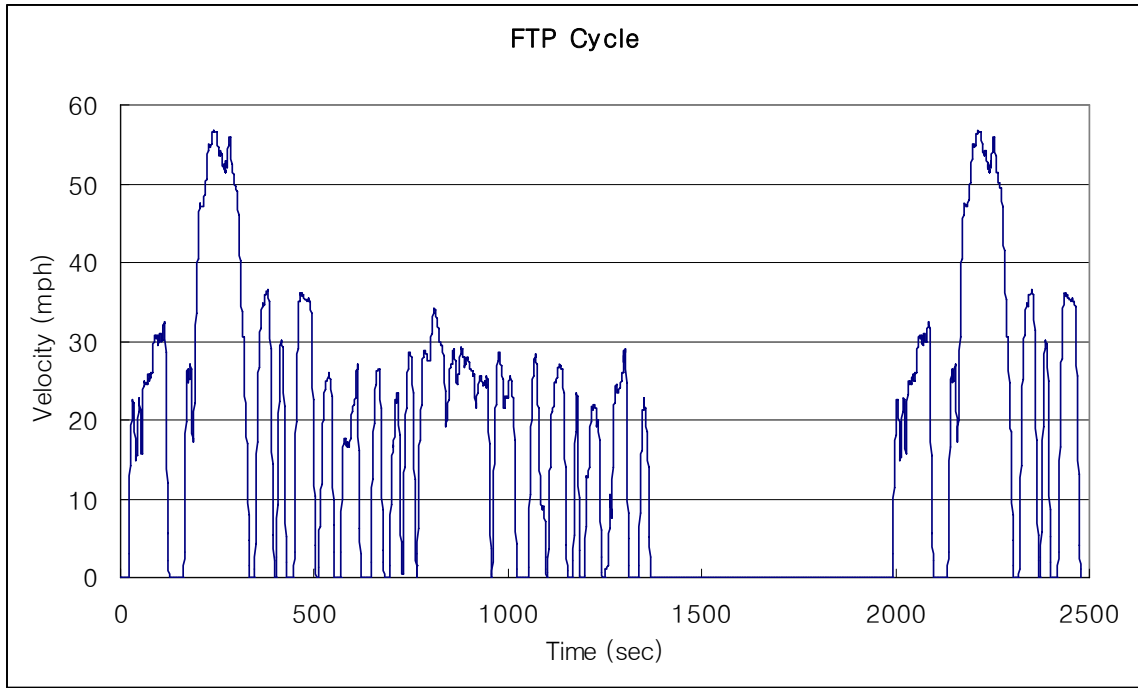


Figure B-3. FTP cycle

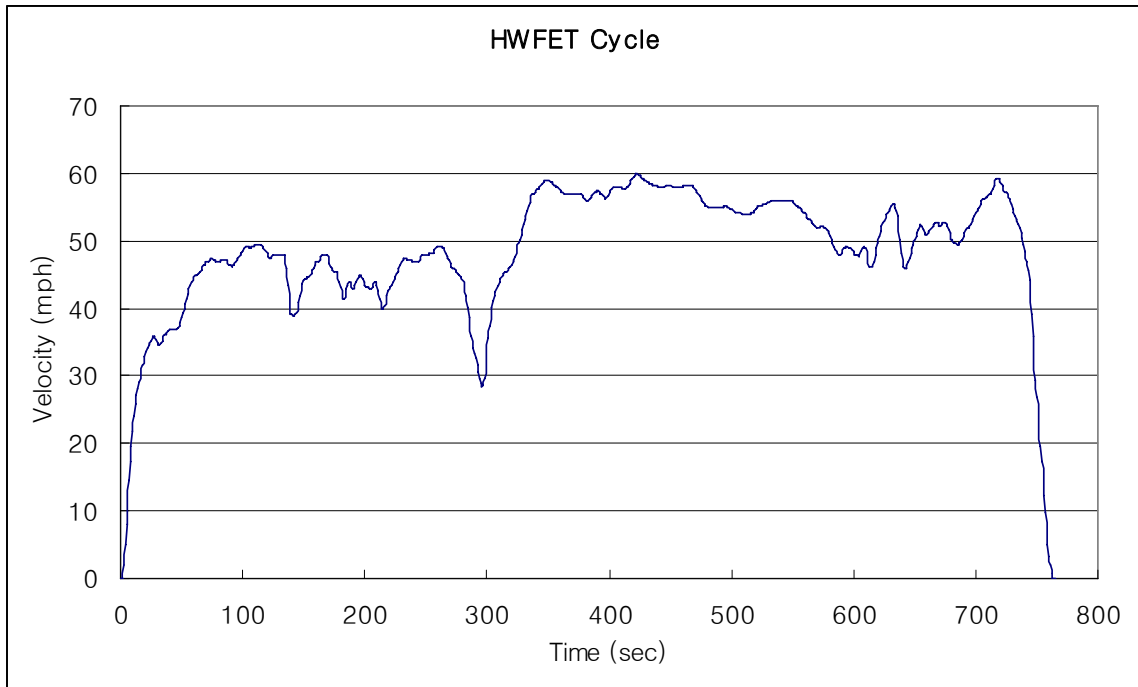


Figure B-4. HWFET cycle

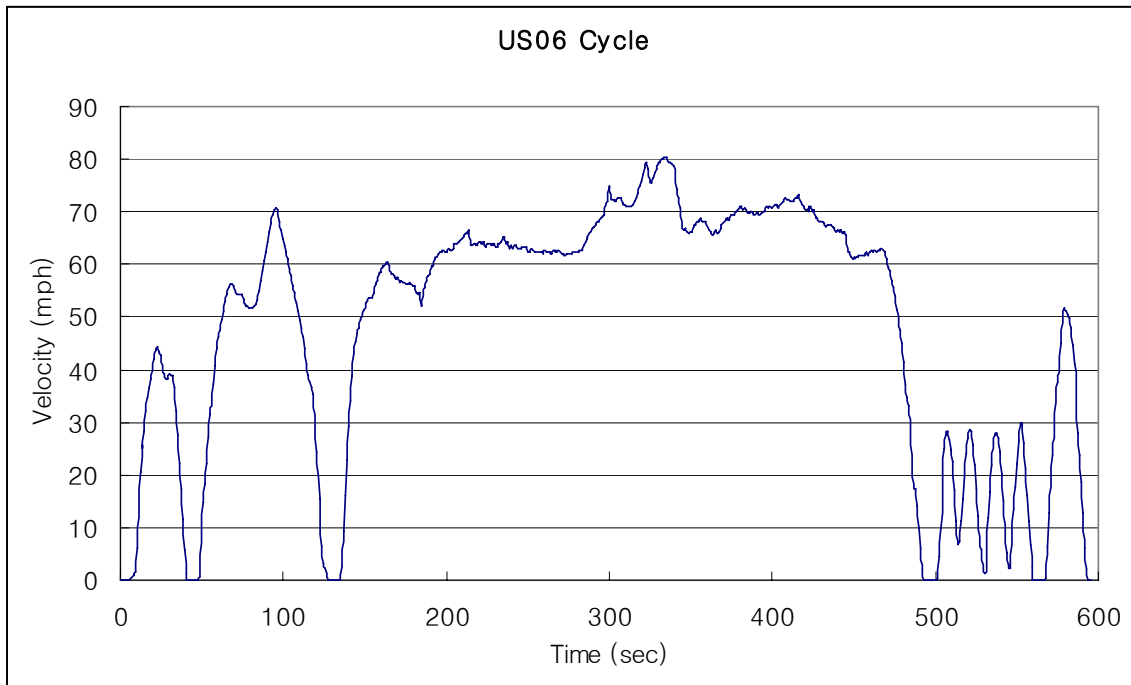


Figure B-5. US06 cycle

Vita

Jeongwoo Lee was born in Suwon, South Korea. He completed his dual bachelor's degree in Mechanical Engineering from both Ajou University, Suwon, South Korean and Illinois Institute of Technology (IIT), Chicago, Illinois in Aug, 2002 and May, 2003 respectively. He joined several senior projects related to vehicle research and the project "NASCAR Technology" was placed first in spring, 2002. He also joined the Caterpillar (CAT) project, "HEUI-B Nozzle Group Redesign - New Types of Nozzle Designs to Reduce or Eliminate the Oil Leakage," with Dr. Herek Clack at IIT, and received an honorarium in spring, 2002. During his undergraduate program, he was awarded a scholarship at Ajou University in his freshman year, 1995, and he had been on the Dean's List for four semesters and earned an IIT scholarship as well. After graduation, he joined M.S. program in Mechanical Engineering at Virginia Tech in Aug, 2003. He performed his research about vehicle performance simulation under Dr. Douglas Nelson's guidance and completed his master's degree in fall, 2005. Jeongwoo Lee is currently pursuing his doctoral degree in Mechanical Engineering at Virginia Tech.